3-11-2011

Combined Effects of Radio Frequency and Electron Radiation on CMOS Inverters

Kristofer R. Dahl

COMBINED EFFECTS OF RADIO FREQUENCY AND ELECTRON RADIATION ON CMOS INVERTERS

THESIS

Kristofer R. Dahl, 2nd Lieutenant, USAF

AFIT/GNE/ENP/11-M03

DEPARTMENT OF THE AIR FORCE
AIR UNIVERSITY

AIR FORCE INSTITUTE OF TECHNOLOGY

Wright-Patterson Air Force Base, Ohio

AFIT/GNE/ENP/11-M03

COMBINED EFFECTS OF RADIO FREQUENCY AND ELECTRON RADIATION ON CMOS INVERTERS

THESIS

Presented to the Faculty

Department of Engineering Physics

Graduate School of Engineering and Management

Air Force Institute of Technology

Air University

Air Education and Training Command

In Partial Fulfillment of the Requirements for the

Degree of Master of Science in Nuclear Engineering

Kristofer R. Dahl, BS

2nd Lieutenant, USAF

March 2011

AFIT/GNE/ENP/11-M03

COMBINED EFFECTS OF RADIO FREQUENCY AND ELECTRON RADIATION ON CMOS INVERTERS

Kristofer R. Dahl, BS

2nd Lieutenant, USAF

Approved:

James C. Petrosky, PhD (Chairman)	4 Mar 11 Date
LTC John W. McClory, (Member)	4 MARCH 11 Date
Gary C. Farlow, PhD (Member)	4 March 2011 Date

Abstract

This research examines the measurement methodology and the results of the combined effects of electron and radio frequency (500kHz) irradiation on a CMOS Hex Inverter, CD4069UB. There have been many studies in recent years on the effects of electron radiation and electromagnetic interference on integrated circuits however the combined effects have not been measured. A major obstacle for in-situ electron irradiation experiments is the over-current hazard that exists to measurement equipment that comes from taking real-time, in-situ measurements. To overcome this, a test circuit was designed and built to allow for real-time in-situ measurement of the output voltage, current and the inverter power. This test circuit provides real–time measurement of the inverter's threshold voltage with respect to electron dose. During this research, pre- and post-irradiation measurements were obtained from an inverter coupled with electron irradiation (1 MeV electrons with fluences up to 8×10^{15} [e^{-}/cm^{-2}] at various fluxes) and a 500 kHz RF signal. The data provided insight into the total dose effect as opposed to a dose rate effect on the inverter. A significant negative threshold voltage shift was observed along with a limited amount of annealing. Inverters that were outliers from nominal VTC characteristics displayed an enhanced failure rate. The combined effects of radio frequency and electron irradiation are inconclusive, but indicate that the RF decreases post irradiation annealing.

To my Lord and Savior, only because of you is this possible. To my wife and kids, thank you for your patience and support over the last year and a half. To my family and friends, thank you all for the constant prayers and encouragement. You all have been such a blessing.

Acknowledgments

The success of this document is due to the constant support and effort of so many people. First and foremost, I would like to thank those on my committee. Dr. Petrosky, thank you for the constant encouragement and guidance, please get some sleep now. To the "Operator of the Dynamitron at WSU", thank you for your time, advice, and patience with all of my "why and how" questions. LTC McClory, thank you for your humor and encouragement through the course of the GNE program. I have been truly blessed to have you three on my research committee,

Without the help of several individuals the experimental portion of this research would not have occurred. Mr. Taylor-AFIT, thank you for willingness to always help every time I had a question and the quick turn-around time for acquiring parts and equipment. Mr. McNeeley-AFIT, thank you for your patience and support by loaning out various pieces of equipment and for your aid with the S_{11} and SWR measurements. AFRL-RASCAL, thank you for allowing me to borrow the RF amp and the ability to test out my equipment in the RASCAL lab. Columbia Engineered Rubber Inc. and Northwestern Tools, without your help the Dynamitron would not have gotten up and running as quickly. AFRL-RYRT, thank you for supplying the signal generator. Finally, thanks to all my fellow classmates. You can finally rest your backs from carrying me for the past eighteen months.

-Kristofer R. Dahl

Table of Contents

Page

List of Figures

Figure Page

Figure Page

Figure Page

Figure Page

Figure Page

List of Tables

List of Symbols and Acronyms

^{60}Co	Colbalt-60
γ	Gamma ray
A	Ampere measure of current
AFIT	Air Force Institute of Technology
BTA	Beam Tube Assembly
CAT5	Category 5
Ci	Curie
CMOS	Complementary Metal Oxide Semiconductor
cm	Centimeter [.01 meters]
CRT	Cathode Ray Tube
dBm	Decibels relative to 1mW
DC	Direct Current
e^-	Electron
EHPs	Electron Hole Pairs
EM	Electromagnetic
EMI	Electromagnetic Interference
EMP	Electromagnetic Pulse
ESD	Electrostatic Discharge
eV	Electron Volt
HPM	High Power Microwaves
Hz	Hertz
I	Current [A]

IC	Integrated Circuit
keV	Kilo Electron Volt [10^3eV]
kHz	Kilo Hertz [10^3 Hz]
LED	Light Emitting Diode
MAC	Mass Attenuation Coefficient
MeV	Mega Electron Volt [10^6eV]
MHz	Mega Hertz [10^6 Hz]
MOSFET	Metal-Oxide-Semiconductor Field-Effect Transistor
NIST	National Institute of Standards and Technology
N_{it}	Interface traps
N_{ot}	Oxide traps
OSURR	The Ohio State University Research Reactor
TI	Texas Instrument
torr	Measure of Pressure (vacuum) torr = 133.3 Pa
rad	Radiation Absorbed Dose
RF	Radio Frequency
RSA	Rectifier Sub Assembly
sec	Second
Si	Silicon
SiO_2	Silicon Dioxide
SF_6	Sulfur Hexafluoride
SMA	Subminiature version A
SMU	Source Measurement Unit

SWR	Standing Wave Ratio
TV	Television
UWB	Ultra Wide Band
V	Voltage
VDG	Van de Graaff
VNA	Vector Network Analyzer
VTC	Voltage Transfer Characteristic
V_{th}	Threshold Voltage
WSU	Wright State University
Ω	Resistance [Ω]

COMBINED EFFECTS OF RADIO FREQUENCY AND ELECTRON RADIATION ON CMOS INVERTERS

I. Introduction

1.1 Problem Description

Collateral damage from military operations creates a ripple effect that dramatically influences the views and opinions of US citizens on military operations [1]. It is the desire of the military to minimize the collateral damage during hostile operation [2]. Therefore, a continuous effort is being made to find ways through technology to finds ways to disable an enemy without causing death. One option is to create a source of intentional electromagnetic interference where this interference has the capability to disable the enemy's technological components. In doing so, it would be advantageous if one could recover these components, ranging from the small computers to large-scale electrical grids.

Various frequencies in the microwave region along with certain power levels have been examined over the past few decades as a means to disrupt and even destroy electronic devices [3]. Along with these frequencies, research has also shown that electron radiation has adverse affects on electrical equipment [4]. However, there has been limited research done in the area of combined effects of the electromagnetic and electron radiation [5].

The underlying purpose of this thesis is to look at such an option of disrupting but not destroying an electrical device by using electrons coupled with radio frequency radiation. If one can understand these effects on the simplest and most common integrated circuits (IC) it would be possible to extend the effects to larger scaled systems.

This process comes at a cost; in-order to understand the effects occurring in the irradiated device, real time in-situ measurements are needed. The term real time refers to measurements taken while the beam of a particle accelerator is on. This is not a pulsed shot, where a device is in-situ, the beam is turned on/off and then a measurement is taken.

In previous research, a gamma ray source of photons was used as the source of irradiation. These photons did not pose an over-current hazard to the measurement equipment [5]. However, if one takes real time measurements while in-situ during electron irradiation, there is the potential that the electrons created from the particle accelerator will couple to the measurement equipment signal lines and destroy the measurement equipment. To overcome this hazard, one has to develop a method of extracting data from a device while being electrically isolated from it. The research presented displays a process for extracting data in-situ, which enhances the understanding of what is occurring in the device during irradiation and provides distinct new opportunities for future research. The ability to take real time in-situ measurements allows one to measure initial effects of the ionizing radiation on a device such as positive trap charge buildup in the oxide versus interface traps. Also, effects may be captured that are missed during pulsed shots, such as damaging current and RF pulses caused by a particle accelerator. Capturing these effects leads to a better understanding of what is occurring and causing disruptions in a device.

1.2 Objective

The purpose of this research is to examine the effects of a specified radio frequency wave combined with a fluence of electron radiation delivered onto a CMOS inverter. In-situ measurements allow one to measure what is occurring during irradiation. Multiple phenomena can be measured, such as positive charge trapping in the oxide and the development of interface traps. Also, it is possible to rule out effects from external sources that may be attributed to the irradiation process, such as beam current or an EMF pulse.

It is expected that the electron radiation will affect the threshold voltage on the inverter, which can in turn change the device logic. An applied RF signal will continue to sustain the electron radiation induced effects even after the radiation source has been removed. This will occur because of the external bias placed on the inverter, which does not allow for the recombination of electron hole pairs.

1.3 Thesis Structure

The thesis is laid out in five chapters. Chapter 2 begins with the CMOS inverter and the reason for selecting it, followed by an explanation of the theory of electromagnetic radiation and its effects on CMOS inverters. Chapter 3 covers the experimental setup, describing how the components allow for in-situ measurements. The procedures are also discussed in chapter 3, while chapter 4 displays the data collected and provides analysis. Chapter 5 summarizes the result and provides future research considerations.

II. Background and Theory

This chapter presents the background and theory of the research. The devices and equipment used for the research are addressed. The device, a CMOS inverter, selected for irradiation will be examined along with its operational characteristics. The theory of electromagnetic radiation is reviewed and then applied to that of electromagnetic interference, describing various types of injection. The section ends with a brief examination of ionizing effects on silicon based devices.

2.1 Device of Interest: CMOS Inverter

The device of interest is the CMOS (complementary metal oxide semiconductor) inverter. According to Sedra and Smith, for any IC technology, the basic circuit element is the logic inverter [6]. Therefore, if one can understand the operation and characteristics of the inverter then the results from it can be extended to the design of logic gates and more complex circuits.

A CMOS inverter is made of two matched enhancement type MOSFETs (metal-oxide-semiconductor field-effect transistor), where one is an n-channel, or NMOS and the other a p-channel, or PMOS. Figure 1 displays a basic diagram of a CMOS inverter. Where V_{in} is the input voltage, V_{DD} is the supply voltage for the inverter and V_{out} is the output voltage. Figure 2 displays a cutaway of a CMOS inverter, showing the p and n substrates.

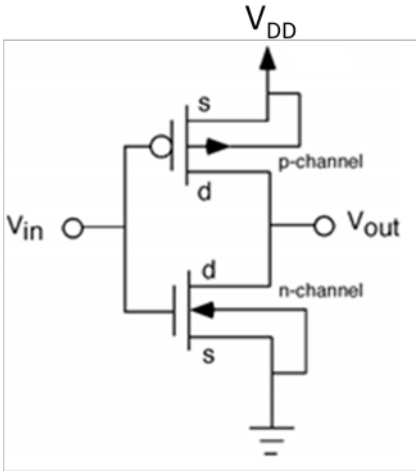

Figure 1. A simple schematic of a CMOS inverter, it depicts the combination of an NMOS (n-channel) and PMOS (p-channel) transistor [7]. When the PMOS is fully on, V_{out} is V_{DD} and when the NMOS is fully on V_{out} is ground.

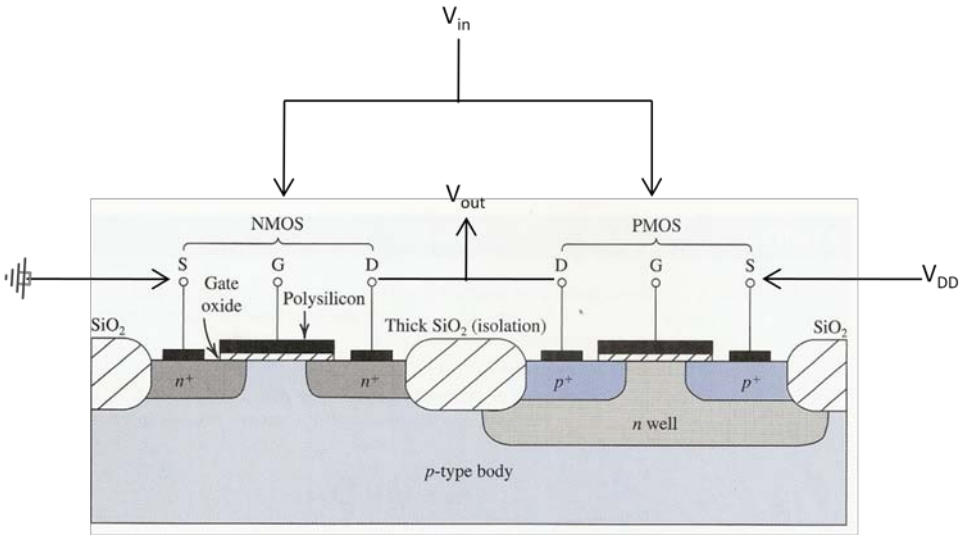

Figure 2. A cutaway of a CMOS inverter [8]. V_{in} is connected to the NMOS and PMOS gates, V_{DD} is connected to the source on the PMOS transistor, while ground is connected to the source on the NMOS transistor. V_{out} connects the drains of both the NMOS and PMOS.

In an NMOS transistor, as a positive bias is applied to the gate, the free holes in the p-substrate are repelled. As the holes in the p-substrate move away from the gate, a depletion region is formed allowing for excess mobile electrons to create a channel below

the gate oxide. When this occurs, a conducting channel is created, where the primary carrier has changed from holes (p) to electrons (n). Because the primary carrier type is inverted, the channel region is referred to as the inversion layer [9]. At this point current is able to flow when a bias is placed across the source and drain terminals. When the bias on the gate attracts a sufficient number of mobile electrons to the channel region, forming a conducting channel, the bias is said to be at the threshold voltage V_{th} [6]. The PMOS transistor works in a similar manner as the NMOS, except the voltage from gate to source is negative, making the threshold voltage negative.

The interaction of how the PMOS and NMOS work under the same bias conditions allows for the operation of the inverter. Table 1 displays the truth table of the inverter. The basic concept is to input a logical 0 and output a logical 1 or vice versa.

Table 1. Truth table for a CMOS inverter.

Input	Output
0	1
1	0

Figure 3 displays a VTC (voltage transfer characteristic) curve showing the state of operations for the PMOS and NMOS transistors. Where V_{DD} sets V_{out} when the input voltage is low, the NMOS is off and V_{out} assumes most of V_{DD}, giving it a high state, which is typically 5 V DC. When the input voltage V_{in} is high, the NMOS transistor is in the on state and the PMOS transistor is off. The channel resistance of the PMOS is higher than that of the NMOS, thus causing V_{DD} to drop mostly across the PMOS and allowing ground to set the output voltage V_{out} [4]. Therefore, the inverter moves from a high to low state, or from a logical 1 to a logical 0 state.

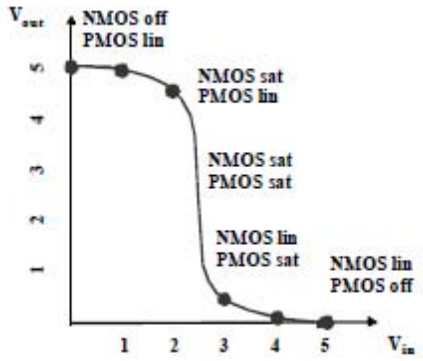

Figure 3. The VTC plot of a CMOS inverter showing the on/off states of a P and NMOS transistors as an input bias is swept from 0-5V [4].

2.2 Electromagnetic Radiation

Electromagnetic radiation is grouped according to the wave frequency. Figure 4 displays the EM spectrum.

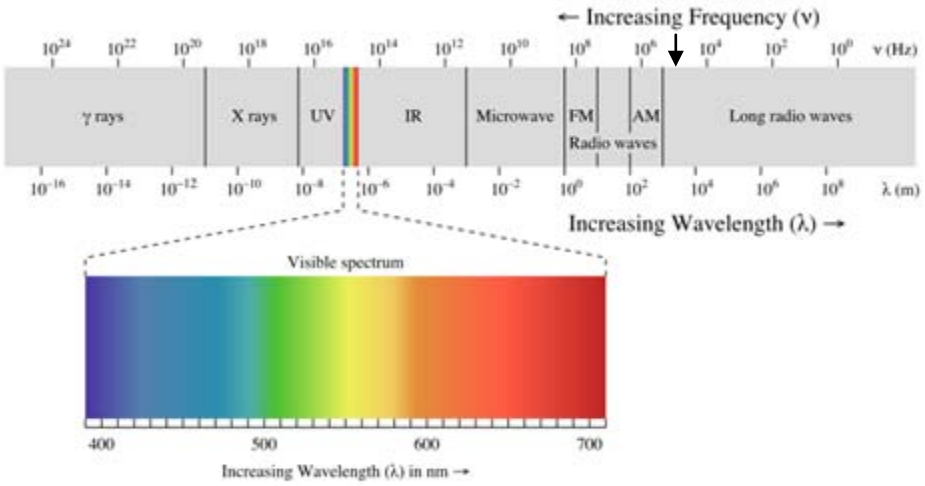

Figure 4. The electromagnetic spectrum, ranging from long radio waves to γ rays [10]. The arrow on the horizontal axis between 10^6 and 10^4 indicates the region of interest for this research.

Ionizing electromagnetic radiation can be defined as a stream of photons; a mass-less, spin 1 particle traveling as a wave and moving at the speed of light. Each photon

contains a discrete energy and all ionizing EM radiation consists of photons. The energy range of these photons defines the high energy EM spectrum [11].

The electromagnetic character of the material and the frequency of the radiation determine the interaction of the radiation with a particular material. According to the Planck-Einstein equation

$$E = hf \,, \tag{0}$$

the energy of a photon can be found where E is the energy, h is Planck's constant, and f is the frequency of the EM radiation [10]. From (1) the frequency of the wave is proportional to the particle's energy. At lower frequencies of radiation such as the radio wave region, the energy will be much lower and therefore not have much of an effect on the material with which it interacts. When the photon energy more closely matches the electronic or molecular energy states of a material, it is more strongly absorbed [12].

By convention, γ rays have their origin in nuclear interactions and x-rays originate from electron or charged particle collisions. Even though the origins are different, the ways these high-energy photons interact with matter are identical. They are lightly ionizing and highly penetrating [13].

2.2.1 Electromagnetic Interference

The EM spectrum has the potential for disrupting electrical devices; this is known as electromagnetic interference (EMI). EMI may occur due to either electromagnetically induced conduction or radiation emitted from an internal or external source. The external source may interrupt, degrade, and possibly limit performance. Internal EMI may be caused from overpopulating a circuit with too many switching devices.

Previous work has shown the ability to create various forms of EMI on devices [14]. Deliberately inducing EMI within a system for the purpose of distorting the signal is known as IEMI (intentional Electromagnetic Interference). Commonly used mechanisms to induce IEMI are:

- High Power Microwaves (HPM)
    - Narrowband
    - Ultra Wideband (UWB)
- Electromagnetic Pulse (EMP)

In the electromagnetic spectrum, microwaves are usually classified as having wavelengths ranging from one meter down to 1 millimeter, with accompanying frequencies of 300 MHz to 300 GHz [15]. The quantum energy of microwave photons is in the range 0.00001 to 0.001 eV, which is in the range of energies separating the quantum states of molecular rotation and torsion. Conductors strongly absorb microwaves at lower frequencies, causing electric currents, which in turn heat the material. Since the quantum energies are a million times lower than those of x-rays, the microwaves cannot produce ionization (with the exception of weakly bonded materials) and the characteristic types of radiation damage associated with ionizing radiation.

In the microwave region, the use of electromagnetic energy has been utilized to induce currents to observe the vulnerabilities of devices. Two methods are used when applying HPM, both narrowband and ultra wide band (UWB). The narrowband waveform has a single frequency with a typical bandwidth of less than 1% of the center frequency. Power is delivered over a fixed period at the single frequency, which ranges

from 100 ns to μs. Experiments have shown some devices to have vulnerabilities in the range of 0.2 – 5 GHz [16].

The other method of applying HPM is UWB, which refers to the energy being produced over a substantial frequency range instead of the single frequency used in the narrowband method. The UWB method is delivered in a repetitive fashion, scanning through various frequencies. With UWB, permanent damage is less of a concern since the energy is distributed over a spectrum of frequencies.

In order to inject HPM, some formal technique must be used to couple the selected frequencies into the intended target. When the HPM is irradiated through the open air with no wires connecting the source to the target, it is referred to as "free space radiation". If the HPM is directly coupled to the system via wires, cables, connectors or any other hardwire conduit, it is referred to as injection. This hard coupling of a system to HPM can be accomplished by two methods, "front door", and "back door."

The front door method is the intended coupling of electromagnetic energy; it may utilize cables and antennas tuned to couple the frequency. The back door is the unintended coupling path of electromagnetic energy where the target may be vulnerable. If a device is poorly shielded it may allow HPM to enter into the system by a variety of pathways, and possibly all at once.

When microwave energy is coupled to components and the energy level is high, damage may occur. This damage can result in increased temperature at junction regions. When the timescale is short compared to that of thermal diffusion times (<100 ns), the temperature may increase rapidly in proportion to that of the deposited energy. In order not to damage the device, care must be taken to ensure that the microwave energy is

below the damage threshold. If one is able to locate the threshold, it may be possible to rectify the microwave energy at the junctions and thus the induced wave will travel like a normal signal with the possibility of temporarily upsetting or disrupting the circuit [17].

EM radiation with frequencies above 100 MHz are capable of penetrating unshielded or poorly protected buildings and cabinets, and therefore being able to couple to electronic equipment inside. However, experiments have shown that EM radiation below 10 MHz propagate more efficiently than those at higher frequencies [16].

Another version of IEMI is from an electromagnetic pulse (EMP). EMP is defined as a burst of electromagnetic radiation that results from an explosion or a sudden power pulse, which causes a fluctuating magnetic field. The wave amplitude (or strength) varies greatly over a broad spectrum from very low to several hundred megahertz, but is mainly in the radio frequency range. Since an EMP can contain a substantial amount of energy, when something inductively couples or absorbs the radiation, that energy is then converted into strong electric currents and high voltages. The relative power density of this signal can be on the order of millions of watts per square meter compared to normal radio waves [18].

2.3 Ionizing Radiation Effects in Silicon

As energetic particles or photons pass through a material, their energy is lost via various interactions and scattering mechanisms. According to Holmes-Seidel, there are two main types of interactions of radiation with materials, atomic displacement and ionization [13]. Atomic displacement occurs when atoms in a material are displaced from their original positions by radiation. The most effective radiation for displacement

damage has a large mass, such as heavy ions like alpha particles. In a silicon substrate atomic displacement damage's primary result is the reduction of minority carrier lifetime. This reduction has a major effect in bipolar devices however, since MOS devices are not normally affected by minority carrier lifetime, they are relatively insensitive to damaged caused by atomic displacement [4].

Ionization occurs when there is sufficient energy to break atomic bonds and create mobile electron/hole pairs (EHPs). In a CMOS inverter, the most sensitive layer to ionizing radiation is that of the silicon dioxide insulator [4]. Research has shown that a net energy of 18 eV is required to create one EHP in SiO_2 [13].

After being produced, a percentage of the EHPs will recombine. If an electric field is present across the oxide it will dramatically reduce the number of recombinations by sweeping the electrons out due to their relatively high mobility in comparison to the holes. At room temperature, the mobility of an electron in SiO_2, μ_n, is $20\left[\frac{cm^2}{V-s}\right]$ compared to the mobility of holes, μ_p, $10^{-5}\left[\frac{cm^2}{V-s}\right]$ [4]. The electrons are swept out of the oxide on the timescale of picoseconds. The holes that escape recombination remain near their point of generation and cause a negative voltage shift in the gate voltage for both PMOS and NMOS transistors. This trapped charge is referred to as oxide trapped charge. Assuming a positive bias is applied to the gate, the holes will move through the oxide towards the interface via a complicated stochastic trap-hopping process. When the holes arrive at the Si/SiO_2 interface they interact with defects, known as hole traps, which results in the formation of interface traps N_{it}. Unlike oxide traps, N_{ot}, interface traps exist

only at the Si/SiO_2 interface and have a significant effect on both recombination rates of carriers at the semiconductor surface and the mobility of the carriers [19].

The number of EHPs created is directly proportional to the amount of energy absorbed by the device material. When ionizing radiation deposits its energy in a device, the valence band electrons are elevated to the conduction band. The creation of these EHPs affect the threshold voltage of a device and a large number of electrons can result in high currents, which will temporarily shut off or turn on a device [20].

III. Experiment

This chapter describes the experimental objectives and methodology necessary to conduct the research. Previous research is addressed and a baseline between the two is formed. Reasons for selection of equipment and devices are discussed, along with the theory of operation being presented. The chapter ends with a detailed explanation of the experimental setup and the procedures used for gathering data.

3.1 Comparison of Research

Previous research has used several methods for injecting IEMI as described in chapter 2, section 2.2.1, such as the examples of UWB and narrowband methods of injecting HPM. Direct injection method was chosen over the free field method for this research in order to have a better controlled environment. An RF signal was used in place of the HPM due to equipment and coupling limitations.

Recently, the effects of RF and γ irradiation on CMOS inverters were examined [5]. A ^{60}Co γ source with an activity of 1212 Ci and maximum dose rate of 73 krad(tissue)/hr was used to irradiate a CD4069UB CMOS Hex inverter. Measurements were taken while the inverters were in-situ at room temperature, along with a concurrent injection of an RF signal [5]. Figure 5 is taken from this work and displays the results of the combined effects of the γ irradiation and the RF signal injected on the inverter. A negative V_{th} shift and downward output voltage trend were observed.

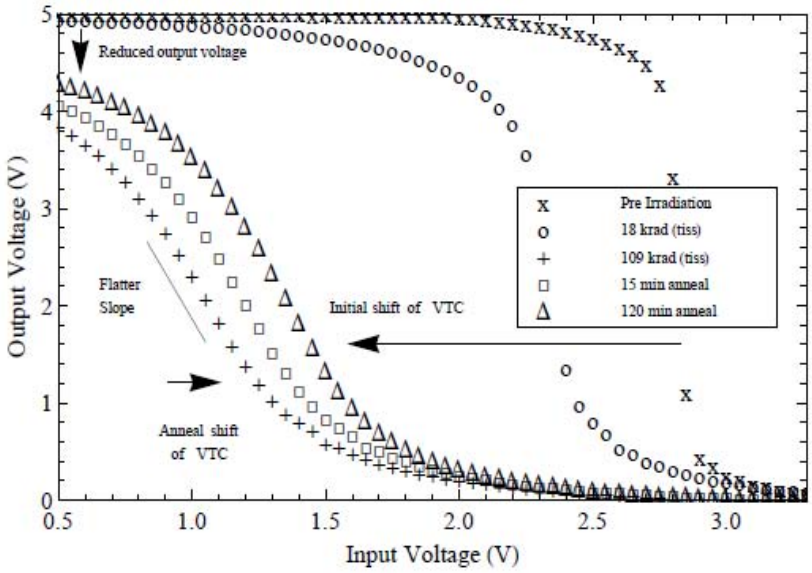

Figure 5. VTC results from combined RF and ionizing radiation during a high input state condition on CD4069UB CMOS Hex inverter. A dose rate of 73 krad(tissue)/hr with a total dose of 109 krad(tissue) conjoined with a 500 kHz 26 dBm HPM signal [5].

For this research, the same version of inverter was used along with the same RF frequency and amplitude, which were coupled with a DC input into the inverter. While previous research results was documented in rad(tissue), this research will document effects with respect to fluence $\left[\frac{e^-}{cm^2}\right]$, in order to aid in conversions related to the electron beam.

A correlation between the total dose used in previous work using γ's and the electron irradiation dose presented in this research must be addressed. The ^{60}Co source is capable of producing two γ's with corresponding energies of 1.33 and 1.173 MeV. From the National Institute of Standards and Technology (NIST) one can obtain the mass energy absorption coefficients (MAC) for the given materials. Using the MACs and known starting dose for tissue, a new dose value can be obtained via equation (2) for the

Si and SiO_2 that are of interest. In equation (2), "$\frac{\mu_{en}}{\rho}$" is the MAC of the material, ρ is the density of the material, D_{eq1} is the known dose, and D_{eq2} is the unknown dose [21]. Table 2 displays the MACs, densities, conversion factor, and the maximum applied dose rate to the given material that was used in previous research [5].

$$D_{eq2} = D_{eq1} \times \frac{\left(\frac{\mu_{en}}{\rho}\right)_2}{\left(\frac{\mu_{en}}{\rho}\right)_1} \tag{0}$$

Table 2. Dose conversion parameters for photon energies around 1.25 MeV [5], [22].

Material	$(\mu_{en}/\rho)[cm^2/g]$	Density $[g/cm^{-3}]$	CF_{tissue}	Maximum Dose Rate
Tissue	2.938×10^{-2}	1.06	1	73 krad(tissue)/hr
Si	2.652×10^{-2}	2.33	0.9	65.7 krad(Si)/hr
SiO_2	4.417×10^{-2}	2.196	1.5	109.5 krad(SiO_2)/hr

A known dose in Si allows correlation to the fluence of a 1 MeV electrons. Figure 6, taken from Holmes-Siedle, provides an energy-dose-to-fluence conversion factor for a 1 MeV electron as 2.45×10^{-8} rad(Si)cm^2. It depicts the following equation

$$\phi = \frac{D}{CF} \tag{0}$$

where ϕ is the fluence in cm^{-2}, D is the total dose in rad(Si) and CF is the conversion factor in rad(Si)cm^2. Once the desired fluence is known, a flux of electrons can be calculated via the known irradiation time and electron beam current; or, through accumulated charge provided by a current integrator.

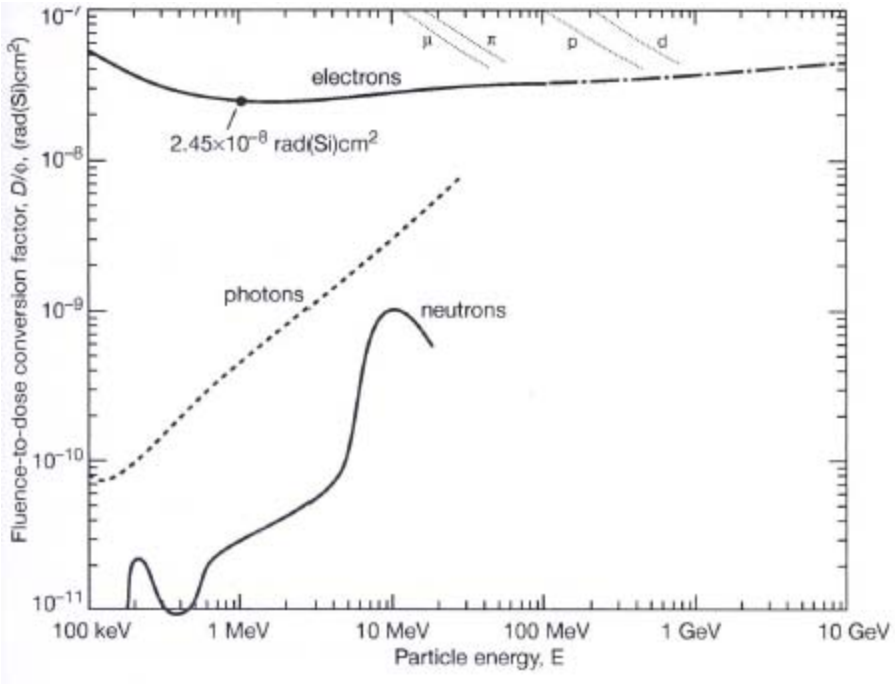

Figure 6. A fluence-to-dose conversion factor for a 1MeV electron [13].

3.2 Selection of Equipment and Devices

In-order for one to be able to make real time in-situ measurements (not pulsed in-situ measurements) of an inverter being irradiated with electrons, the inverter should be electrically isolated from the measurement equipment. If this does not occur, there is the possibility that the electrons from the electron accelerator will couple to the signal wires on the inverter being irradiated and migrate back to the measurement equipment. This excess current may provide a false signal or worse, result in damage to the equipment. The following section describes the inverter selected for irradiation, the electron accelerator, the measurement equipment, and the test circuit that allows for protection for the in-situ measurement.

3.2.1 CMOS Inverter

A Texas Instruments CD4069UB Hex Inverter was chosen for irradiation. This style of inverter has been well documented in previous research [23], therefore its performance under irradiation has been well established, providing a means to verify the experimental approach [5]. Using the same inverter in this research allowed for a comparison of the effects caused by the two sources of irradiation at dramatically different dose rates. Figure 7 displays the schematic of the inverter and the pin layout. It consists of 6 PMOS-NMOS transistor pairs, for a total of 12 transistors. Of the 14 pins, 12 correspond to inputs and outputs for the PMOS-NMOS pairs while the remaining 2 pins are for power input and ground [24].

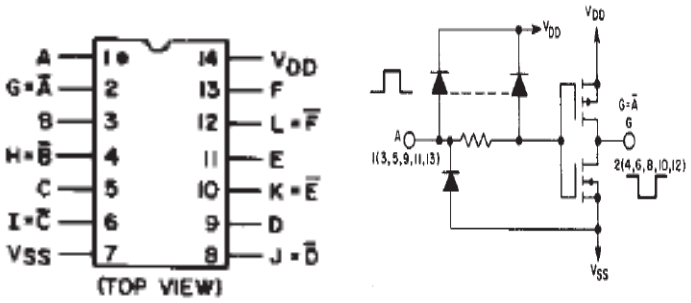

Figure 7. (Left) A pin assignment, where V_{DD} is positively biased and V_{SS} is negatively biased, an example of input/output pin assignments is pin 10 is an input while pin 2 is an output. (Right) internal schematic of TI CD4069UB Hex inverter [24].

3.2.2 Electron Accelerator

An electron accelerator works similar to that of a CRT (cathode ray tube). The electrons are generated from a heated filament [25]. A voltage gradient draws the electrons away from the filament and accelerates them through a vacuum tube.

The electron accelerator chosen for this research was a Dynamitron model EA 1.5. The Dynamitron can provide a 0.5 to 1.5 MeV constant potential electron beam with

a controllable current from 0 to 10 mA and a maximum power of 15 kW at a full potential of 1.5 MeV. It uses a cascaded solid-state rectifier system that operates from an RF AC power supply [26].

The Dynamitron is made up of three major components: a High Voltage Accelerator Assembly, an RF Power Oscillator Assembly and a Control Console Assembly. The High Voltage Accelerator Assembly converts relatively low voltage RF energy to an extremely high DC potential. The nominal 220 V AC is rectified and converted into RF energy of 10 kV at a frequency of 300 kHz, which is fed into the Toroidal Coil Assembly and the RF Electrode Section. The Toroidal Coil Assembly and RF Electrode Section behave as an autotransformer and boost the RF signal to approximately 150 kV peak-to-ground. At this point, the signal is then applied to the Rectifier Sub-Assembly (RSA), which allows the signal to be converted up to a 1.5 MV DC current.

The RSA is made up of several solid-state rectifiers that are connected in series between ground and the high voltage terminal. They are positioned in two columns on opposite sides of the Beam Tube Assembly (BTA). The BTA is a hollow cylindrical tube that is 48” long and is sealed within the pressure vessel. The BTA and rectifiers are surrounded with hollow metal tubes that act as corona shields; corona being an electrical discharge caused by the ionization of the insulating gas, which surrounds the BTA, and presents a hazard to equipment. These corona rings have two distinct roles; the first is to suppress sparks and corona discharge from the rectifier terminals. While its second role is to provide a large surface capacitance for coupling the radio frequency power to the rectifiers. The RSA is encapsulated in a sealed pressure vessel that is filled with SF_6

(sulfur hexafluoride) gas at high pressure. The SF_6 has two roles. First, it prevents sparking and corona discharge from the corona shields to the resonant electrodes. The second role of the gas is to act as a dielectric between the resonant circuit (Toroidal Coil Assembly and RF Electrode Section) and the rectifiers, which provides DC insulation and AC coupling.

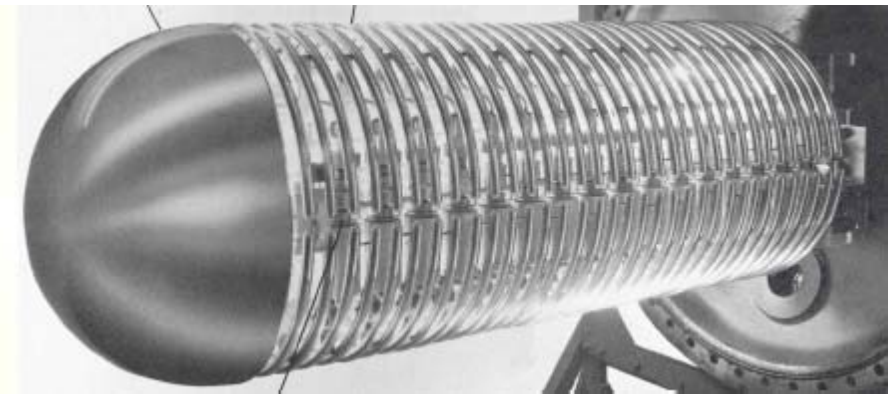

Figure 8. The Dynamitron, showing corona rings wrapping around the rectifiers, inside lays the beam tube assembly [26]. The above picture is encapsulated by the pressure vessel (not shown), which is filled with SF^6.

As the RF signal propagates along the corona rings, the rectifiers see a DC signal that is equal in amplitude to that of the RF signal. The rectifiers are in series, which allows the signal at one rectifier to add to the next one, thus allowing for a maximum potential voltage of 1.5 MeV.

The BTA is under the vacuum pressure of approximately 3×10^{-7} torr before the start of an electron shot. This situation allows for the electrons to travel efficiently down the beam tube. The BTA is made up of a series of glass spacers and dynodes. The dynodes are a highly resistive breeder network under high voltage that keep the electron

centered in the beam while the glass spacers provide insulation and prevent electron scattering.

As the electrons emerge out of the end of the pressure vessel, a scan magnet is used to help align the beam. AC power is used for the scanning process, while DC power is used for directivity of the beam in the x and y direction.

The electrons begin at the filament inside the pressure vessel in which a process similar to that of the CRT occurs. The electrons are drawn from the filament by a relatively low voltage potential, ~ 10 kV, into the BTA. This is an emission current and is adequately described by the Richardson equation [27]. As the electrons travel down the BTA, they continue to see a higher voltage potential at each rectifier, which increases their speed. As the electrons emerge out of the BTA and continue down the beam tube, the electrons no longer see a high potential due to the beam tube being grounded. The electrons continue to move forward with little beam divergence due to their relativistic speed. The scan magnet is used at this point to correct any misalignment that may be occurring in the beam [12]. Eventually the electrons collide with a cold head, which is electrically isolated from the beam tube. The electrons flow through a Brookhaven BIC 1000C current integrator, which was set to a sensitivity of 1 count per 200 nC. These counts, representing accumulated charge, allow one to determine fluence and flux of the beam.

3.2.3 Bias T

In previous research [5], a Mini-Circuit ZX85-12G bias T was used to couple the input DC signal of the inverter to an RF signal. For this research, the RF will not be coupled to the DC via the bias T, however the bias T will still be used as a source of

protection from any DC current resulting from the Dynamitron's e-beam. Figure 9 displays a schematic of the bias T used. In the figure, a capacitor can be seen in line between the RF/RF&DC ports. This capacitor will block any DC returning current that may couple to the signal line.

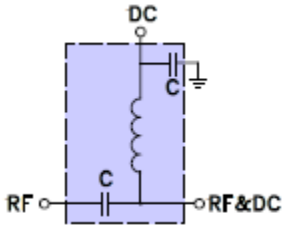

Figure 9. A schematic of the bias T used to provide protection from any return DC [28].

3.2.4 Optoisolators

Various methods were examined for electrically isolating the inverter from the measurement equipment during irradiation [29]. Optoisolators were determined to be an effective way of isolating the inverter from the measurement equipment. The following section describes how the optoisolators function, depicting how they provide electrical isolation while maintaining a capability to take measurements.

An optoisolator works by means of an optical interface. An LED (light emitting diode) and a phototransistor are enclosed in a light, tight container with no electrical connection between the two of them. The LED side is connected to the source side of the circuit. When current passes through the LED, it brightens, emitting photons, which are then detected by the phototransistor [30]. The phototransistor has an extra large p-type semiconductor region that is open for light exposure. As the photons created by the LED interact with electrons in the p-region, the electrons gain enough energy to migrate across

the p-n junction energy barrier. As the electrons leave the p-region, holes are created. The extra electrons injected into the lower n-type region are drawn toward the positive battery terminal, while the electrons from the negative side of the battery terminal recombine with the holes. The result is a net electron current that flows from the collector to the emitter [30].

In order to remain electrically isolated, a separate voltage source provides power to the phototransistor side. Figure 10 displays the circuit inside the optoisolator.

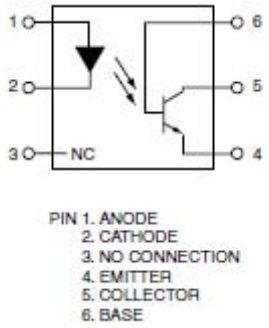

Figure 10. Schematic of the internal operation of an optoisolator and the corresponding pin layout [31].

Figure 11 displays the input versus output voltage of an optoisolator with the collector voltage being varied. As the collector voltage is increased, the output window of the optoisolator is also increased. Figure 11 shows the optoisolator delay in turn on voltage and a steep linear region slope.

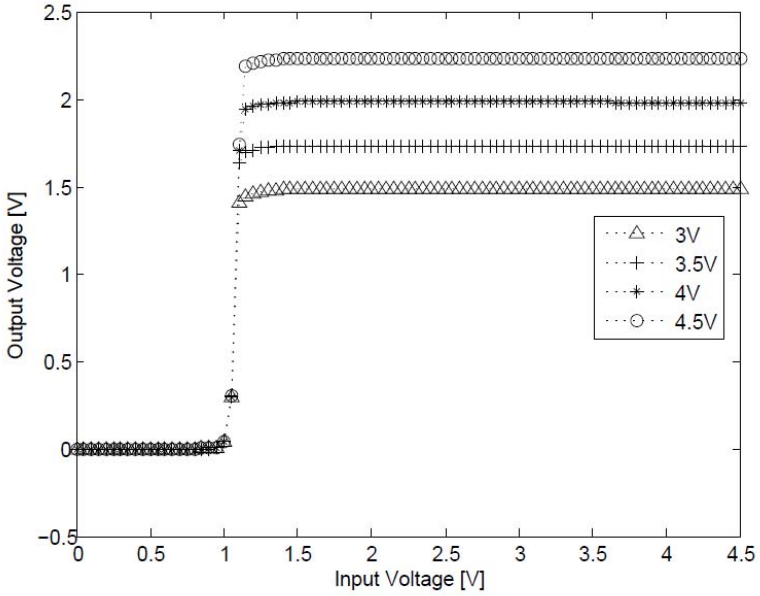

Figure 11. Optoisolator input versus output voltage with varied collector voltage. The output voltage of the optoisolator increases proportionally with the increase in collector voltage.

As the optoisolator quickly moves from a zero to a one instead of a gradual increase, the inverter will quickly shift from a one to a zero. This quick shift is problematic if the V_{th} of the inverter is required to be sampled. To allow for a gradually increasing linear region, a resistor is placed in line with the LED side of the optoisolator with input port 2. The result is displayed in Figure 12. The collector in Figure 12 is held at 9.6 V produced via a battery sourcing the right side of the optoisolator.

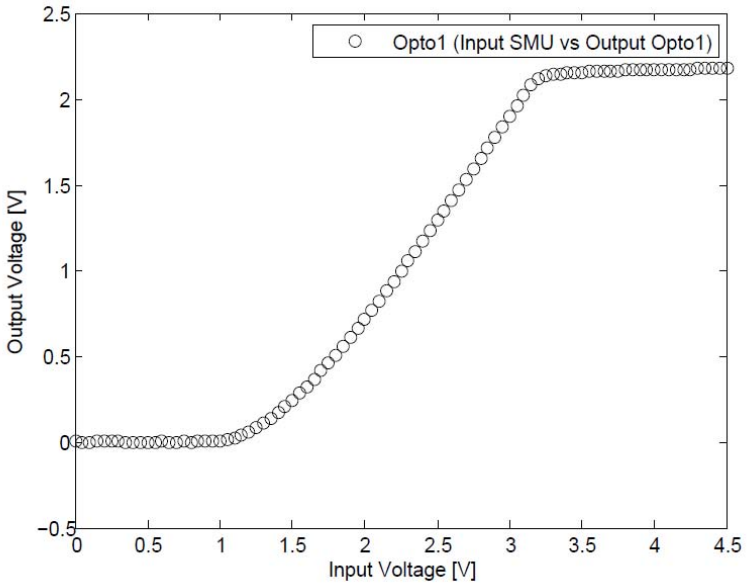

Figure 12. A 1k resistor placed on LED side of optoisolator, creating a gradual increasing linear region in the output voltage.

3.3 Test Circuit Design

A test circuit was built in order to isolate electrically the measurement equipment from the inverter, while being irradiated. This test circuit allows one to take real time, in-situ measurements during electron radiation of an inverter. Two versions of this test circuit were designed and fabricated. The first, which will be referred to as test circuit A, uses only one 9 V battery and is completely floated, while the second, referred to as test circuit B, uses two 9 V batteries and ties the inverter side to the Dynamitron ground.

Figure 13 presents the schematic for the test circuit A, the area labeled II indicates that it is electrically isolated from the measurement equipment via two optoisolators. A Keithley 4200 is used to both measure and source the inverter, located in area's I and III in Figure 13. It was selected due to its versatile capability of being integrated with three source measurement units (SMU). One SMU (area I) will sweep the first optoisolator

from 0 to 4.5 V, which creates the input voltage for the VTC plot. As current is passed through the first optoisolator, its LED begins to emit light, thus producing photons and turning on the phototransistor. Since the right side of optoisolator 1 (area II) must be electrically isolated from the equipment it cannot be sourced with an SMU. Therefore, a 9 V battery is used in order to float the power to the optoisolator's collector. A second battery is used to power the inverter through the input V_{DD} port. The batteries allow for protection from any accumulated charge produced on the inverter while being irradiated by the Dynamitron. Since charge moves towards the point of lowest potential, the accumulated charge will dissipate to earth ground and not to the floating ground.

As SMU 1 is swept from 0 to 4.5 V, a threshold voltage is reached and the input on the inverter goes from a logic zero to a logic one. Simultaneously, the inverters' output goes from a logic one to a logic zero.

An RF signal is produced by an Agilent E4438C ESG Vector Signal Generator (area I) and then passed through an RF amplifier ZHL-32A to boost the amplitude of the signal to the desired power of 26 dBm. The amplifier is powered via a DC power supply at 23 V. The RF signal is passed through the bias T described in section 3.2.3, then couples with the DC signal from SMU1 at the input leg of the inverter (area II). The bias T could not couple the RF signal as in previous research [5] with the input DC, due to the input DC being floated, while the RF signal was earth grounded causing a mismatched system. Therefore, the bias T's purpose is to act as a DC block for any unwanted DC signals produced from the Dynamitron that may couple with the signal lines. The current produced from the inverter output will activate the LED on optoisolator 2, thus enabling the phototransistor for that optoisolator. A second SMU (area III) will provide power to

optoisolator 2's collector, while a third SMU will read the output voltage from the emitter of that optoisolator.

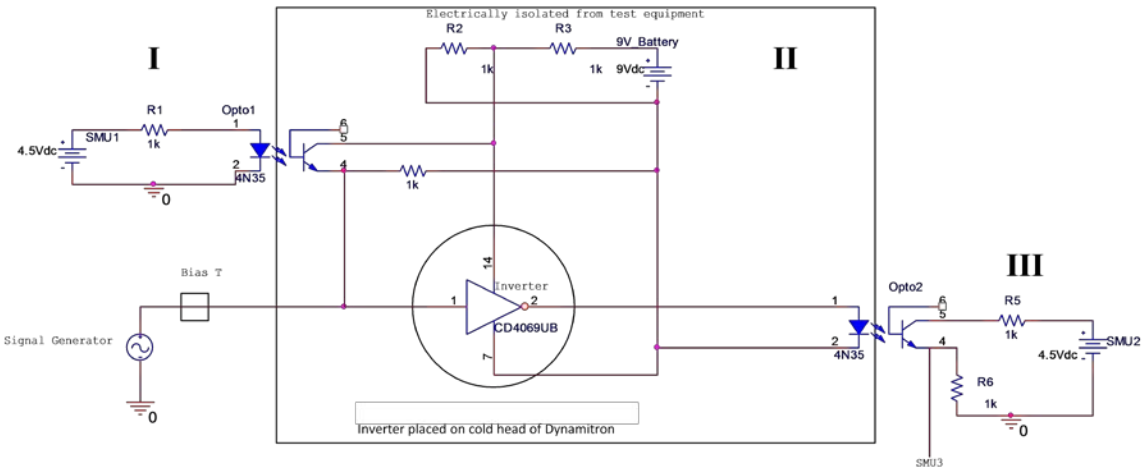

Figure 13. Schematic of test circuit A, where area II is electrically isolated from areas I and III. Voltage is swept from 0 to 4.5 V by an SMU in area I, while two SMUs measure and source in area III. A 9 V battery sources both the inverter and the optoisolator 1 in area II.

Figure 14 displays the schematic for test circuit B. Note the second 9 V battery (area II) and leads being tied to the Dynamitron ground. A second battery was used to increase the voltage on the collector of optoisolator 1, allowing for a larger output range. On the isolated side, ground leads connect the battery's ground to the Dynamitron ground. While this does put the optoisolators and inverter at risk from any current or RF pulses created from the Dynamitron's beam and/or high voltage, the test circuit is still electrically isolating the measurement equipment from the inverter. By grounding to the Dynamitron ground any accumulated charge on the inverter/cold head is able to dissipate thus giving a more accurate measurement.

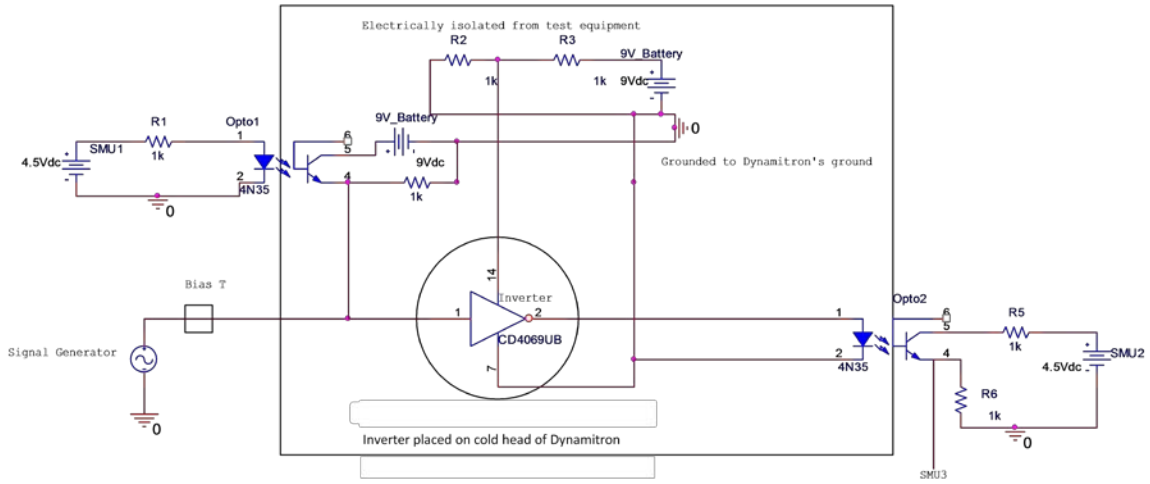

Figure 14. The schematic of test circuit A, where area II is electrically isolated from areas I and III. Voltage is swept from 0 to 4.5 V by an SMU in area I, while two SMUs measure and source in area III. Two 9 V are used in area II, one to source the inverter, while the other to source optoisolator 1.

3.4 Setup

The Dynamitron lies within an underground room surrounded with concrete walls known as the exposure room. Lead-lined wooden doors allow access from the control room to the exposure room. Access ports permit cables to be passed from the exposure room to the control room and are configured in such a way to minimize radiation leakage. To ensure the measurement equipment would not be harmed by the x-rays produced by the Dynamitron, the equipment was placed outside of the exposure room in the control room. Figure 15 shows the layout of the two rooms while Figure 16 shows the equipment.

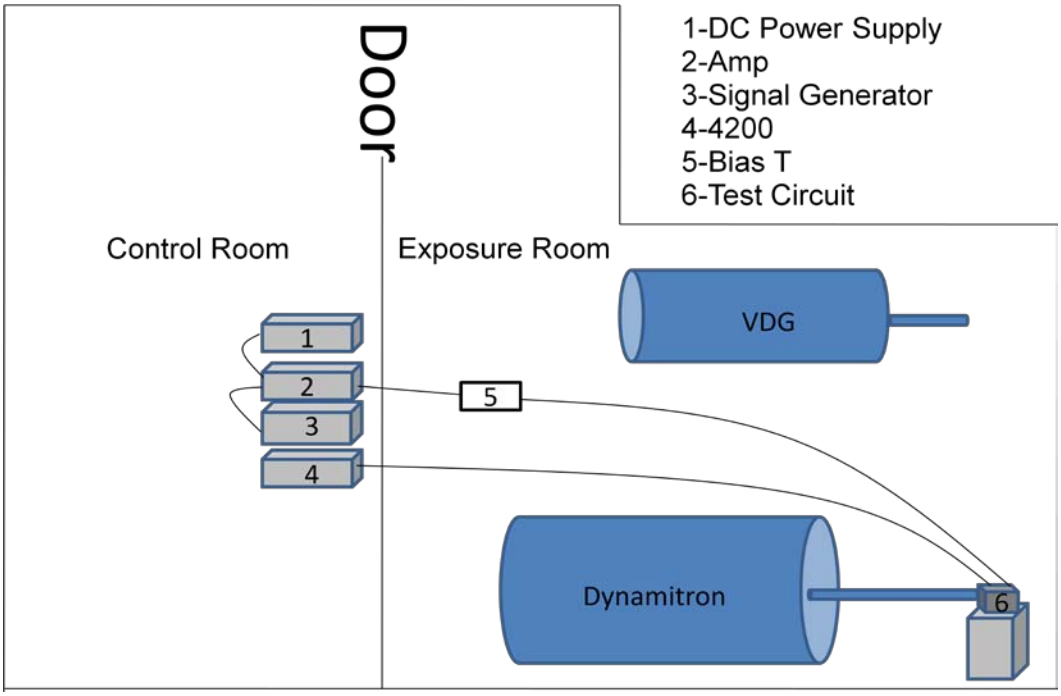

Figure 15.The layout of equipment in control/exposure room at WSU (not to scale). All measurement equipment was located outside of the exposure room in the control room. The test circuit, inverter and bias T were located in the exposure room. A CAT 5 and SMA cable were used to provide and receive signals from the inverter.

A CAT 5 cable passes the DC signal between the Keithley 4200 and the inverter. A sub-miniature version A (SMA) cable carries the RF signal from the signal generator to the inverter. The RF signal connects to the same input leg of the inverter as the DC input voltage from SMU1. Figure 17 presents the signal flow of the experiment.

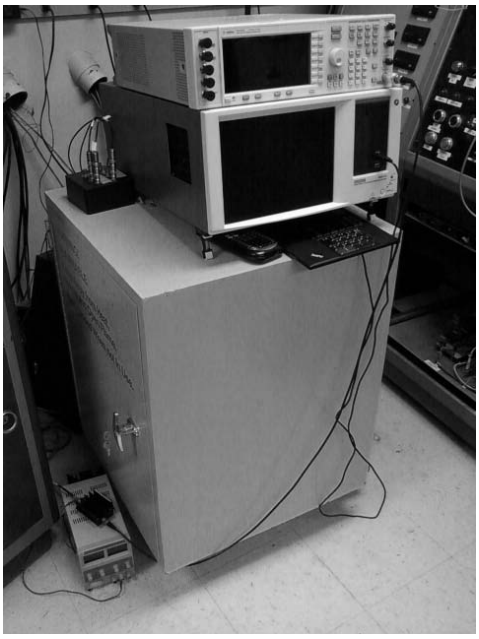

Figure 16. Measurement equipment located in the control room. On the floor (left), DC power supply with RF amplifier resting on top. On the workbench (bottom) the Keithley 4200 with signal generator on top. A signal control box (sitting to the left of the 4200) was designed to pass signals to and from the 4200 onto the CAT 5 cable.

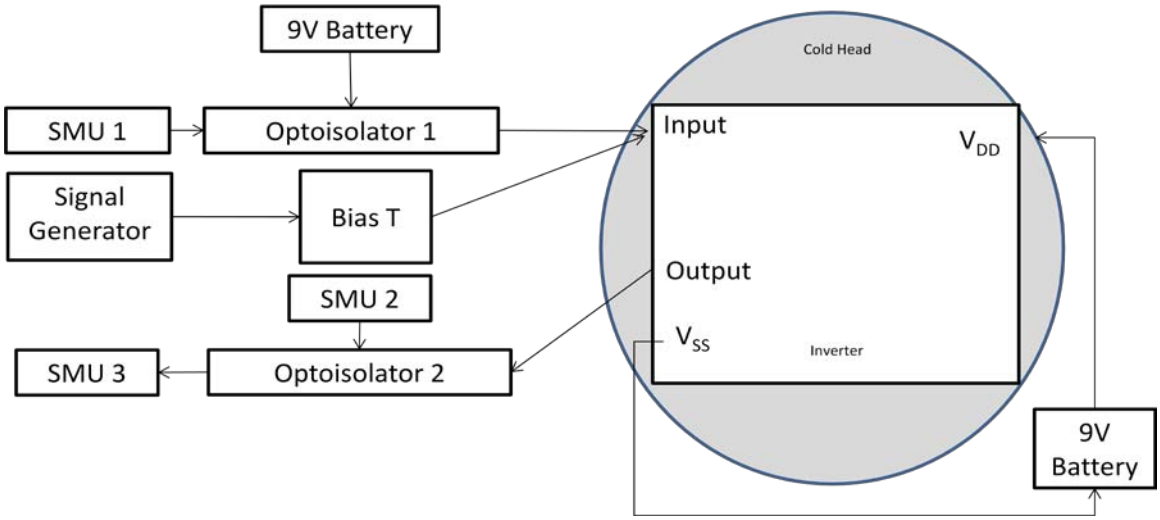

Figure 17. Signal flow of measurement equipment, test circuit and inverter (not to scale).

A cold head seals the beam tube on the Dynamitron. The inverter is placed on the cold head, which is then inserted into the beam tube assembly to be irradiated under

vacuum. The cold head serves several purposes. First, it acts as a mount for devices to be placed into the beam tube of the Dynamitron. Once connected to the beam tube, it creates a seal, allowing for vacuum pressures of $\approx 3\times10^{-7}$ torr to be reached. Under this vacuum, electrons are able to travel down the length of the BTA without energy attenuation. Cooling tubes are passed through the inside of the cold head to aid in cooling the device being irradiated. The cold head is electrically isolated from the beam tube via a Viton gasket and nylon bolts. By allowing the cold head to be electrically isolated from the beam tube, a current integrator can be used to determine the electron fluence as described in section 3.2.2 above.

A collimator was built to filter out electrons that were not travelling parallel to the beam tube, thus allowing for the beam spot area to be characterized. The collimator is displayed in Figure 18. It is inserted into the beam tube in front of the cold head. A piece of clear plastic was mounted to the cold head and then irradiated. Using the electron induced darkening, the beam spot area was measured as 5.3 cm^2.

Fluence was calculated by first finding the charge using equation (4),

$$Cnts \times F.S. = [C] \tag{0}$$

where Cnts is the number of counts from the current integrator and F.S. is the sensitivity setting of the current integrator. From the charge one can find the number of electrons by

$$\frac{[C]}{q\left[\frac{C}{\#e^-}\right]} = \#e^- \tag{0}$$

,

where q is the fundamental charge. Finally, fluence can be found by

$$Fluence = \frac{\#e^-}{Area} \tag{0}$$

,

where #e $^{-}$ is the number of electrons calculated from equation (5) and area is 5.3 cm^2 as determined by the beam spot characterization. The flux was similarly calculated by using equation (7),

$$Flux = \frac{\frac{\#e^{-}}{\sec}}{Area}. \quad (0)$$

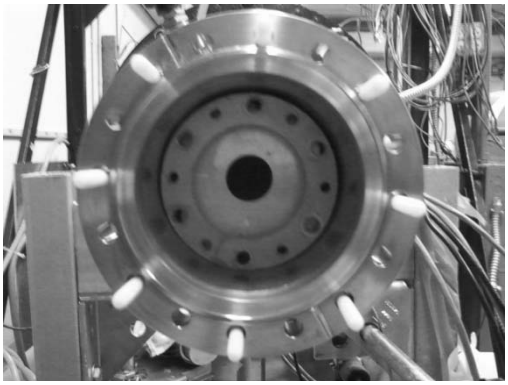

Figure 18. The collimator rests inside of the beam tube, where it is used to characterize the beam spot area. Nylon bolts are used to electrical isolate the cold head (not shown) from the beam tube and can be seen protruding out the end of the beam tube.

In-order to reduce connection capacitance and heating damage from soldering, the measurements and supply wires were connected to the legs of the inverter via a wire wrapping method, as shown in Figure 19. These wires were connected to the test circuit, which reside outside of the cold head. The test circuit was shielded from x-rays with an aluminum block as displayed in Figure 20.

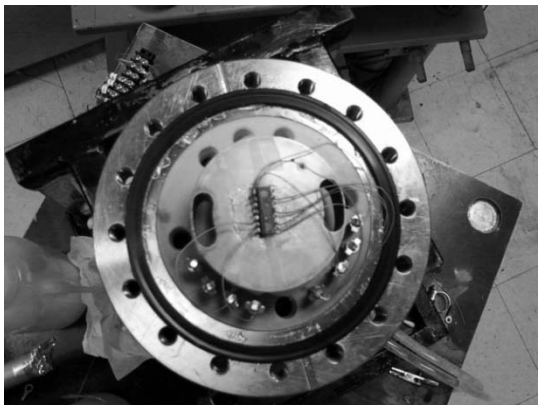

Figure 19. An inverter placed on the cold head. The legs of the inverter are attached to wire by wire wrapping. The wires are then connected to the terminal post, allowing for signals to be passed through the cold head.

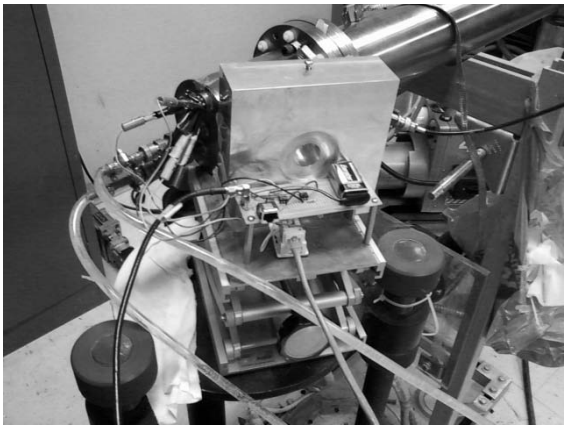

Figure 20. The test circuit, showing CAT 5 and SMA connections, floating battery and connection from the test circuit to the cold head. An aluminum block shields the test circuit from radiation produced from the Dynamitron. Cooling tubes are connected through the back of the cold head, which are filled with de-ionized water that is cooled via a chiller.

3.5 Procedures

All inverters to be irradiated were pre-characterized and compared to manufacture specifications. A process similar to previous research [5] was used, as follows:

1. Pre-characterized inverters

2. Measure RF coupling: SWR and S_{11} measurements taken to verify if the RF signal would couple into the device.

3. Measure RF effects on inverters
4. Measure electron effects on inverters
5. Measure combined effects of RF and Electron irradiation on the inverters.

The inverters were mounted and irradiated one at a time while on the cold head of the Dynamitron. A small amount of vacuum grease held the inverter in place on the cold head. Each leg of the inverter was wire wrapped, and connected and a functional check was performed with the device inside the cold head, to ensure the correct connections and to provide a noise baseline. Once mounted, the cold head was attached to the beam tube and then the beam tube was placed under vacuum pressure. When the correct pressure was reached, another functional check was performed on the inverter.

During RF measurements, the RF signal was applied before the beam was turned on. It was left on for the duration of the irradiation and removed after the beam was turned off. Once the beam was turned on, the beam current was applied at low levels, starting around 10-30 nA. It was then gradually increased and reached currents as high as 2 μA.

IV. Results and Analysis

This chapter provides the analysis of the results from the in-situ measurements. It describes the pre- and post-irradiation and the combined in-situ measurement results. The chapter begins by addressing the measurements of the coupling efficiency of the RF signal to the inverter using SWR and S_{11} measurements.

Terms used throughout the chapter are defined as follows. The waveform is the sourced voltage wave generated during the in-situ measurement at optoisolator 2 (inverter output) during a transition from high to low as observed from the Keithley 4200. Waveform shifting is when something occurs in the inverter to change the waveform baseline from 0 volts. When a large step change occurs, the waveform is no longer in its original shape, which is not shifting. The PMOS-on and NMOS-on (output high and output low respectively) sides of the waveform are in reference to Figure 3 in section 2.1. When the inverter is held in the high state, the input legs not attached to the input voltage from SMU1 are connected to V_{DD}, which is the high side of the battery. Similarly, when the inverter is held low, the other inputs are connected to V_{SS}.

4.1 RF Coupling Efficiency

In order to find an efficient coupling frequency, a standing wave ratio (SWR) and S_{11} measurement was performed on the inverters. An HP87720C vector network analyzer (VNA) was used to take these measurements. Due to limitations of the VNA the lowest frequency that could be addressed was 50 MHz. The VNA swept the frequency from 50 MHz to 3 GHz. The inverter was connected as it would be for the experiment such that the VNA was connected to 45' of SMA cable through the bias T into the test

circuit, which was connected to the cold head with the inverter mounted. Figure 21 and Figure 22 display the results for the SWR and S_{11}.

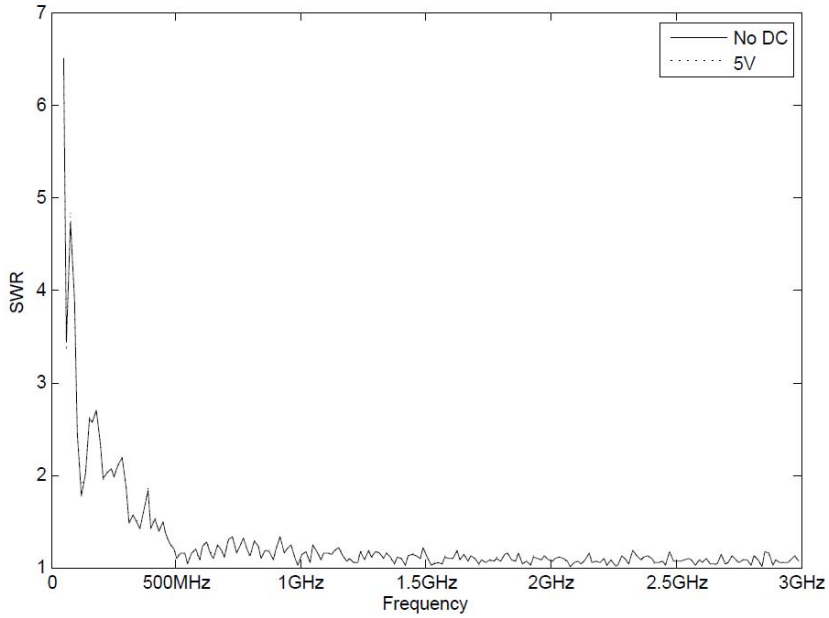

Figure 21. SWR measurement with inverter mounted to cold head, indicating the signal attenuation. The frequency is swept from 50 Mhz to 3 GHz, while power is supplied to the inverter.

Figure 21 demonstrates that for low frequencies, the SWR is largest. Around 125 MHz the SWR drops below 2:1, which indicates a more efficient coupling of the RF signal. The SWR appears to improve as the frequency approaches 500 MHz and is stable thereafter. However, this does not mean the signal is coupling with the inverter effectively, as much of the signal is attenuated at these higher frequencies, which reduce the reflecting wave. Figure 22 shows a similar effect around the 500 MHz region, where a resonant coupling frequency exists. As with the SWR measurement, this is likely due to the attenuation of the RF signal. In previous research [5], a resonant frequency of 850 MHz was measured during the S_{11} measurement. However, when the RF signal was coupled with the inverter input no effects were measured. It was likely that the inverter

did not reflect the RF signal, but attenuated it. This was resolved by mounting the inverter to a PCB (printed circuit board). A larger response was measured around 500 kHz while coupled to the input DC signal. Since the inverter is placed under vacuum, use of a PCB is not possible due to out-gassing. Therefore, the same 500 kHz frequency was used as in previous research [5].

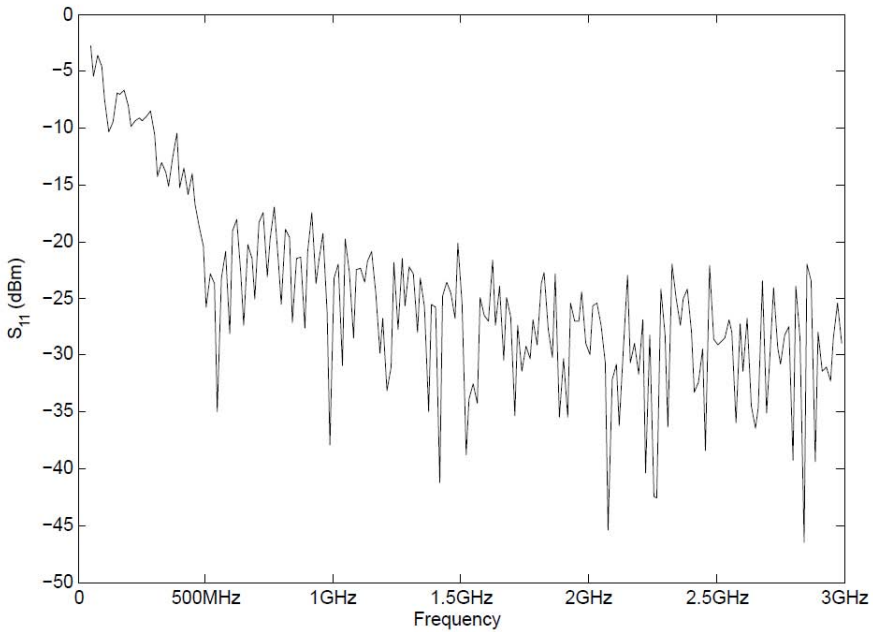

Figure 22. S_{11} measurement of inverter mounted to the cold head, indicating the signal attenuation. The frequency is swept from 50 Mhz to 3 GHz, while power is supplied to the inverter.

4.2 Inverter Response to RF and Electron Irradiation using Test Circuit A

4.2.1 Pre-Irradiation VTC (Pre-VTC) Measurements

Before irradiation, the inputs of the inverter were held high (V_{DD}) and then low (V_{SS}) for one minute in order to obtain a baseline VTC measurement for each device. Figure 23 displays a nominal pre-VTC response, showing an overlap of the high and low input measurements.

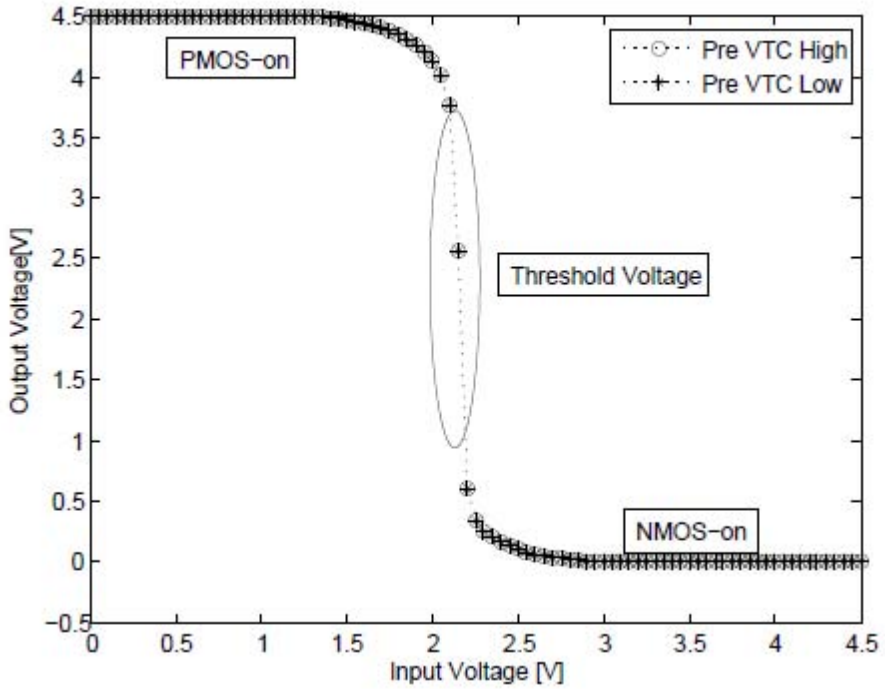

Figure 23. For the pre-irradiation VTC, the input legs of the inverter are held in a high (V_{DD}) or low (V_{SS}) state and a VTC measurement is taken. Results of the high and low states show an overlap in the VTC curve. The P and NMOS transistor "on" region are displayed along with the threshold voltage (V_{th}).

4.2.2 Electron Irradiation: Inverters Held High

An in-situ measurement of an inverter with no RF applied was initially made to create a baseline for a combination measurement of electron irradiation coupled with an

RF signal. Figure 24 presents the in-situ measurement during irradiation. The electron current was slowly increased from 300 nA to 2 μA. Care was taken not to pulse the inverter, which may cause very high dose damage to the device, such as punch-through or breakdown. As the fluence increased, the output voltage of optoisolator 2 decreased. Larger downward output voltage shifts were noted between waveform measurements as the dose and current increased. A steady decrease in output voltage occurred when the beam current was above 1 μA. The NMOS-on side appeared to be more sensitive to changes when the current increased above 2 μA. This can be observed as the NMOS-on side voltage of the waveform was reduced to 0 V.

The voltage reduction in Figure 24 on the NMOS-on state is due to a floating ground. Since the NMOS references ground is the negative terminal of a battery, it allows for the gate to be higher than the system reference. As charge begins to accumulate, it creates a ground path within the inverter. This charge build-up causes the waveform baseline to decrease steadily. The PMOS-on state of the waveform in Figure 24 begins to decrease due to decrease in the input of optoisolator 2. The inverter's output voltage supplies the input voltage for optoisolator 2. The decreased input voltage can be attributed to the PMOS not fully turning on.

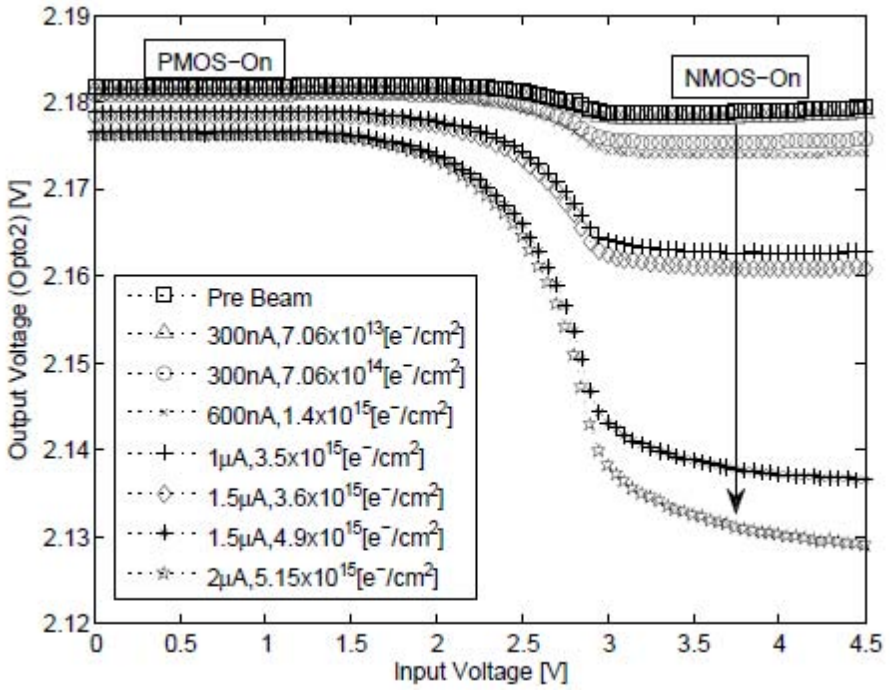

Figure 24. In-situ measurement of an inverter being held high, no RF was applied. Various flux levels were obtained throughout this measurement. A small output voltage shift is noted on the PMOS-on side, which is contributed to the PMOS not fully turning on. While a larger shift is noted on the NMOS-on side, which is contributed to charge that has accumulated within the inverter creating a ground path.

Figure 25 shows the waveform through optoisolator 2 before the electron beam is turned off. It shows the beam being turned on and the waveform as current is increased to 2 μA and the resultant waveform before the beam is turned off.

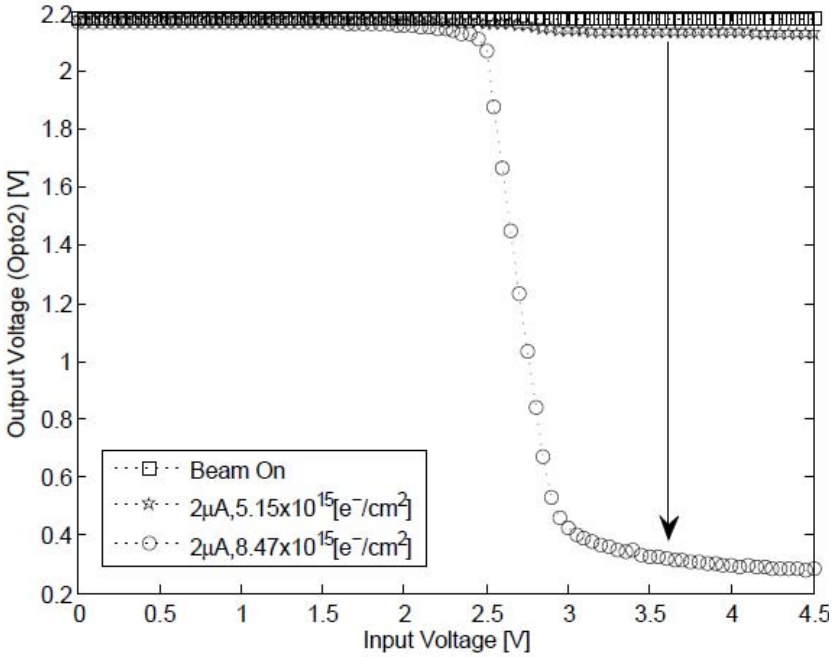

Figure 25. In-situ measurement of inverter being held high, no RF applied. The figure presents that larger charge accumulations occur at higher fluences.

Figure 26 shows an increase in output voltage on the NMOS-on side of the waveform after the electron beam has been turned off. The waveform was measured continuously for 9 minutes afterward and presented a steady rise in output voltage.

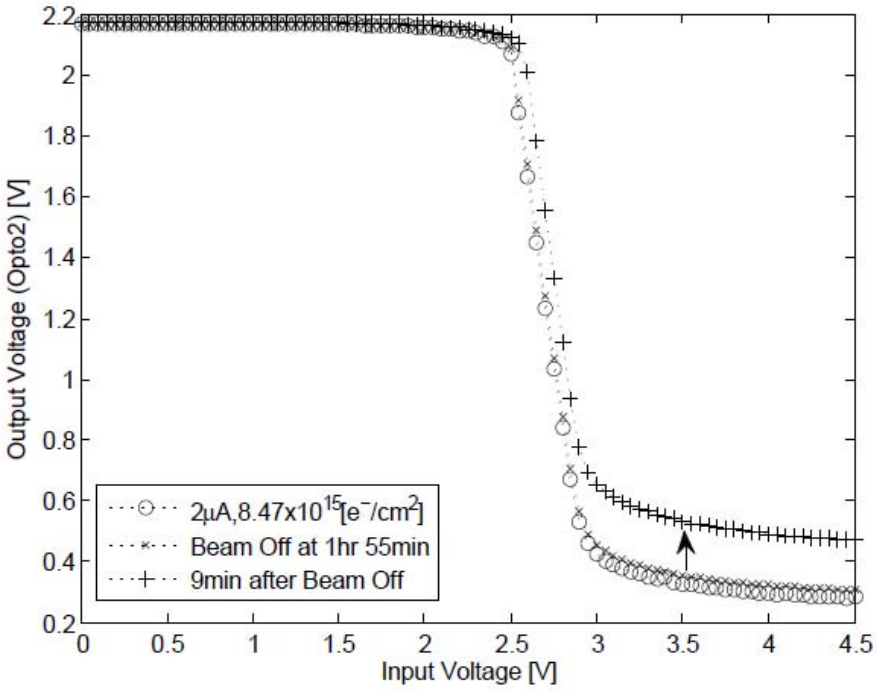

Figure 26. A measurement of the final fluence before the beam was turned off, the beam off after irradiation, and 9 minutes after the beam was turned off. A recovery of the waveform post irradiation is noted, which is due to the dissipation of accumulated charge.

Figure 27 presents the pre- versus post-VTC. All inputs are held high during the measurement. The first post-VTC measurement was completed 20 minutes after the electron beam had been turned off. A negative V_{th} shift is observed when compared to the pre-VTC. Another post-VTC measurement was taken 25 hrs later, indicating a slow annealing process.

The negative V_{th} shift that took place in the inverter is caused by the creation of EHPs in the oxide. The lower V_{th} indicates that the PMOS is switching to an off state and the NMOS is switching to an on state much earlier. This is due to the accumulation of holes in the oxide, therefore requiring less of a bias on the gate to switch.

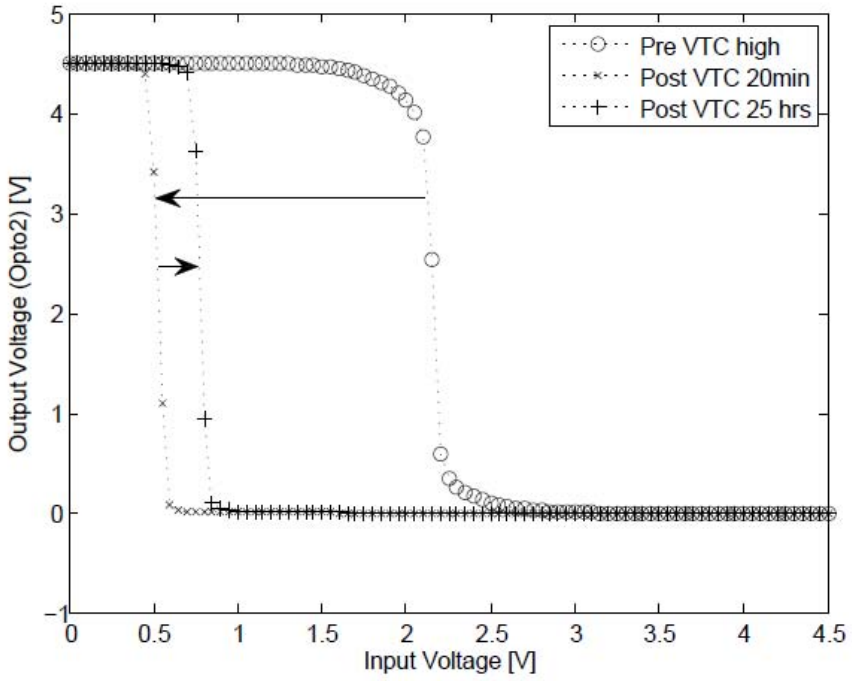

Figure 27. Pre-versus post-VTC of inverter held high with no RF applied, showing a negative V_{th} shift, along with some annealing.

4.2.3 Electron and RF Combined: Inverter Held High

The irradiation procedures used in section 4.2.2 were repeated on another inverter. This time a 500 kHz RF signal with an amplitude of 26 dBm was applied with the DC voltage to the input leg of the inverter before the beam current was turned on. By monitoring the inverter output pre-irradiation and comparing it to the output during irradiation allows for compensation of the beam RF coupling to the inverter. The beam current was initially set at 300 nA and increased up to 2 μA. The RF signal was held constant for the duration of the irradiation and remained on for 10 minutes after the beam was turned off. Figure 28 shows the result of this measurement and shows similar results to that of Figure 24. Once the RF is applied, the waveform reduces the output voltage, as measured through optoisolator 2.

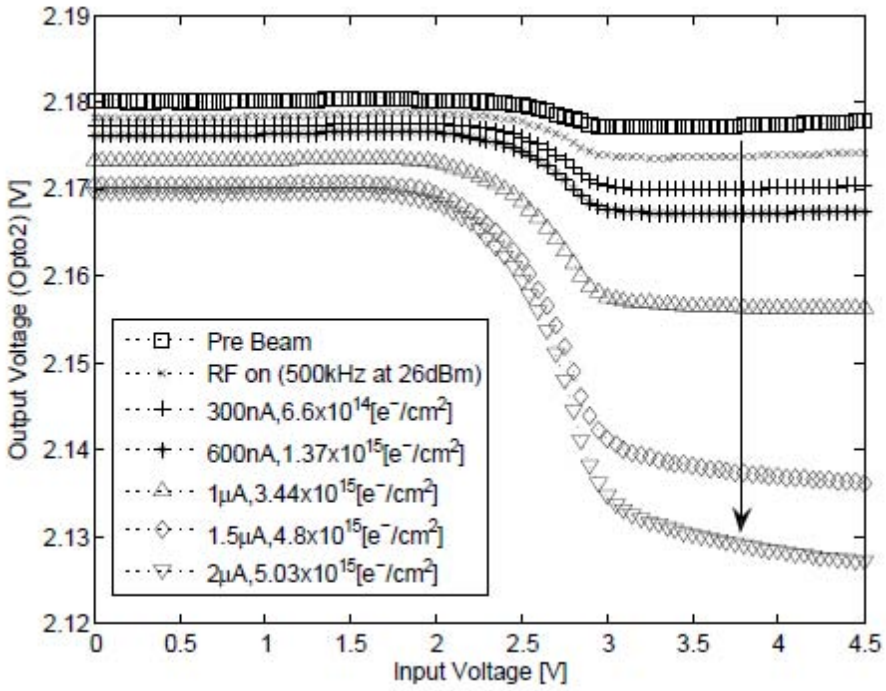

Figure 28. Inverter held high, irradiated via the same process as in section 4.2.2, but with an RF signal at 500 kHz with an amplitude of 26 dBm applied. Similar results were obtained with a small shift in PMOS-on compared to NMOS-on states.

In Figure 29 the inverter was irradiated to a total fluence of 9.53×10^{15} [e^-/cm^2] as compared to the fluence of Figure 24 at 8.47×10^{15} [e^-/cm^2]. However, similar effects were observed around the same fluence and current levels when no RF was applied.

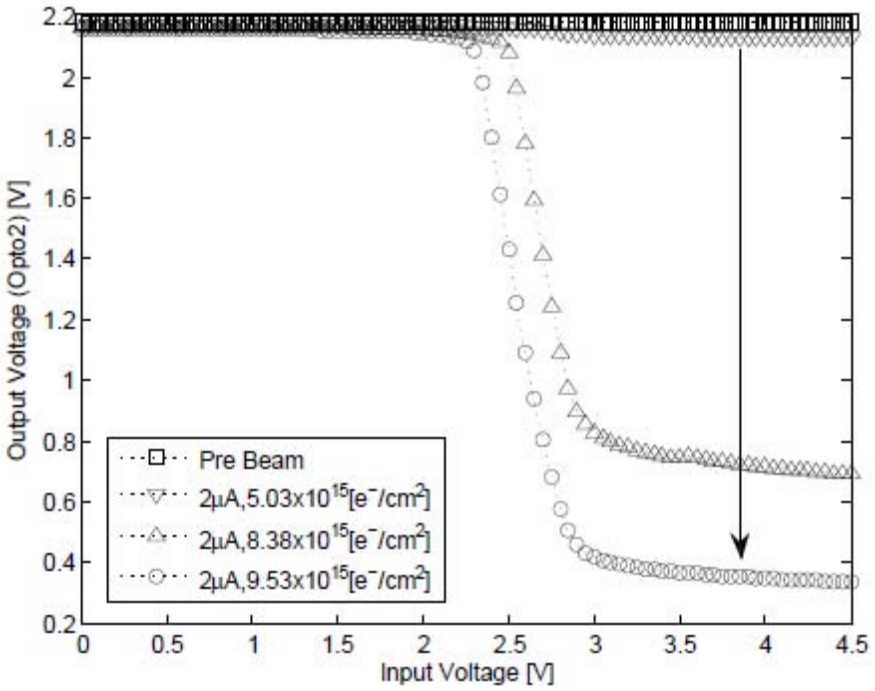

Figure 29. Inverter held high, irradiated via the same process as in section 4.2.2, but with an RF signal at 500 kHz with amplitude of 26 dBm applied. The figure presents the larger charge accumulations occurring at higher fluences.

Figure 30 presents the final fluence measurement before the end of irradiation. The RF signal remained on afterward, causing an increase in the output voltage similar to that shown in Figure 26 when no RF signal was applied. After ten minutes, the RF signal was turned off, responding as shown in Figure 30.

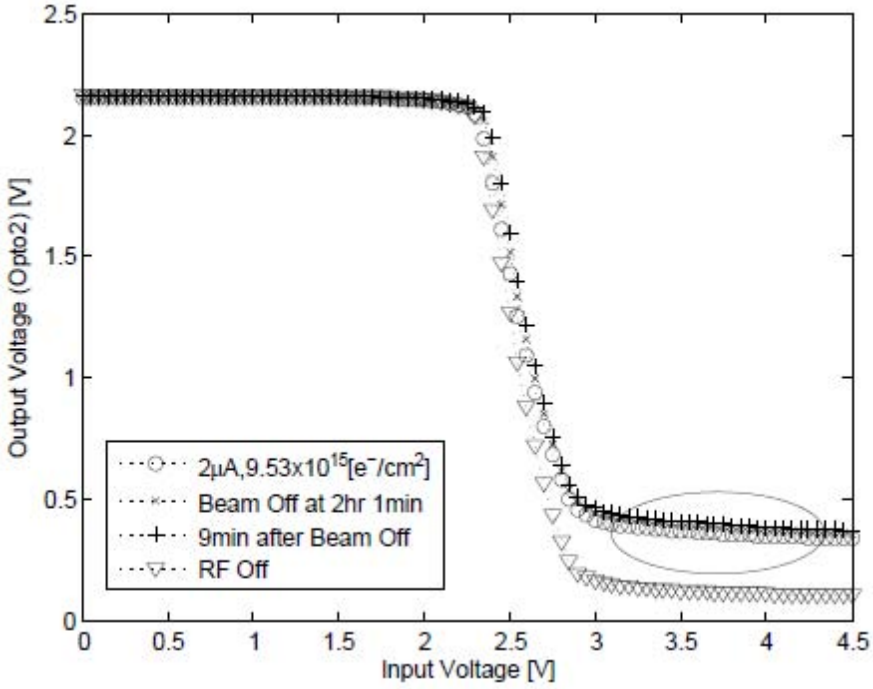

Figure 30. Inverter held high, post irradiation measurement with RF still applied (ellipse area). After RF is removed the waveform shifts to a lower output voltage.

Figure 31 presents the pre- versus post-VTC response, showing a similar result as in Figure 27.

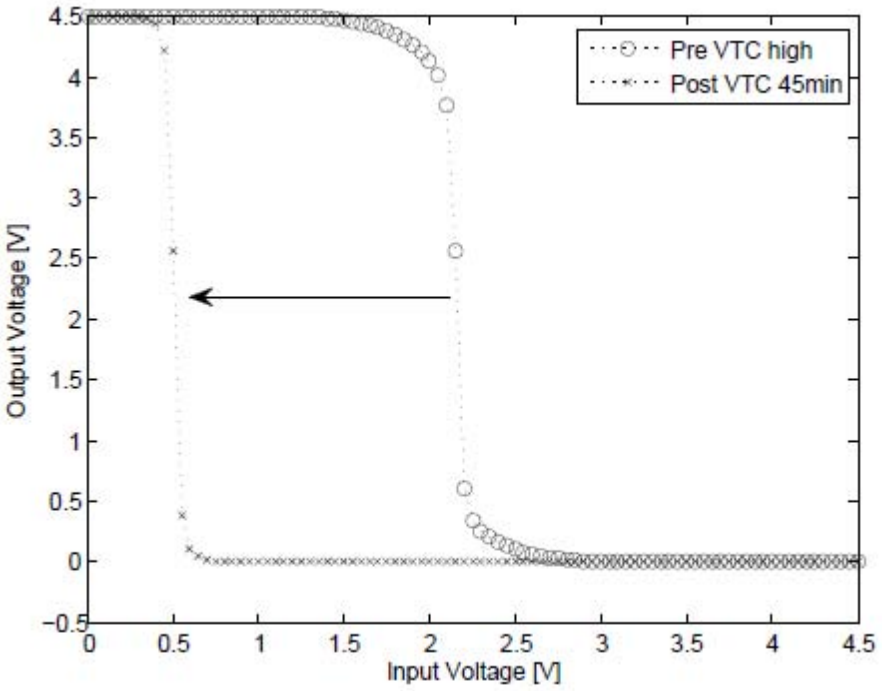

Figure 31. Pre- versus post-VTC of inverter held high with an RF applied. There was no observable difference to V_{th} with and without RF applied.

4.2.4 Radiation Effects on Outlier Inverters

The term "outlier" refers to those inverters whose response did not match the nominal pre-irradiation VTC response as shown in Figure 23. Two cases are presented; the inputs were held low and the inputs were held high. Figure 32 presents the pre–VTC response. The V_{th} shifts positive from the nominal inverter position of ~2.25 V. This indicates that the PMOS transistor is held in the "on" state for a longer time and the NMOS transistor does not turn on fully.

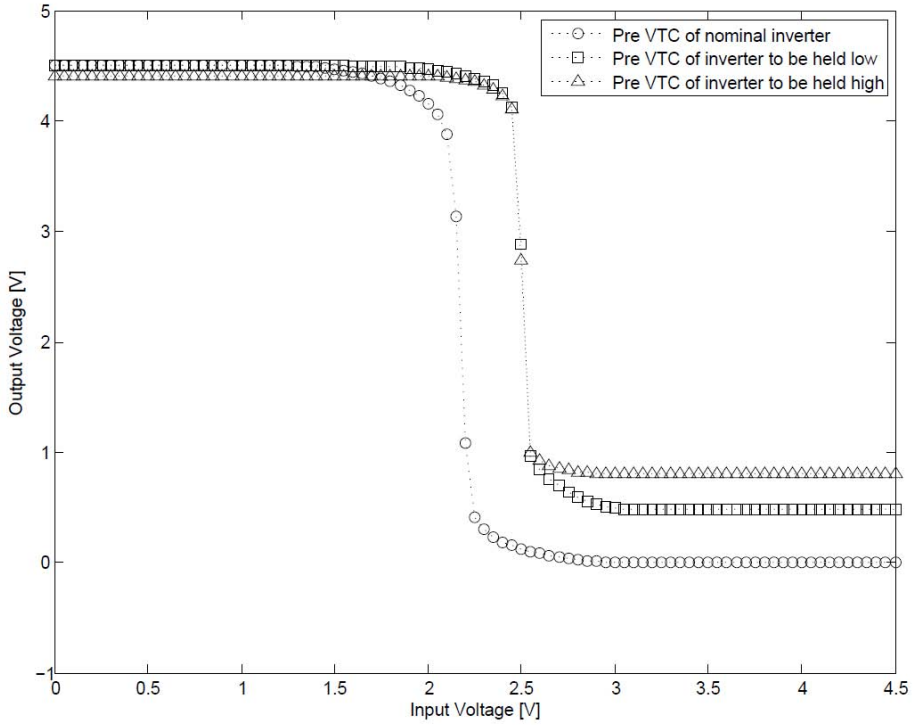

Figure 32. Pre-VTC of outlier inverters, presenting a positive V_{th} shift from the nominal VTC threshold voltage.

The inverter in Figure 32 was measured with the inputs held low during irradiation with an initial beam current at 150 nA and monotonically increasing it to 400 nA. Current spikes were observed during this irradiation through the current integrator. These spikes may have been a cause for an observed change in output at ~38 minutes. Following irradiation, a post-VTC measurement was made showing that the inverter response was most like the nominal VTC response as seen in Figure 33.

In Figure 32 the inverter was held high. It was irradiated for 6 minutes before a change occurred. The beam current was initially at 30 nA and was increased to 550 nA. Several current spikes were also observed during this measurement. As shown in Figure 33, the post–VTC response of this inverter did not return. In this situation, the PMOS

transistor is remaining in the “on” state during a transition for much longer, and the NMOS transistor does not turn on fully.

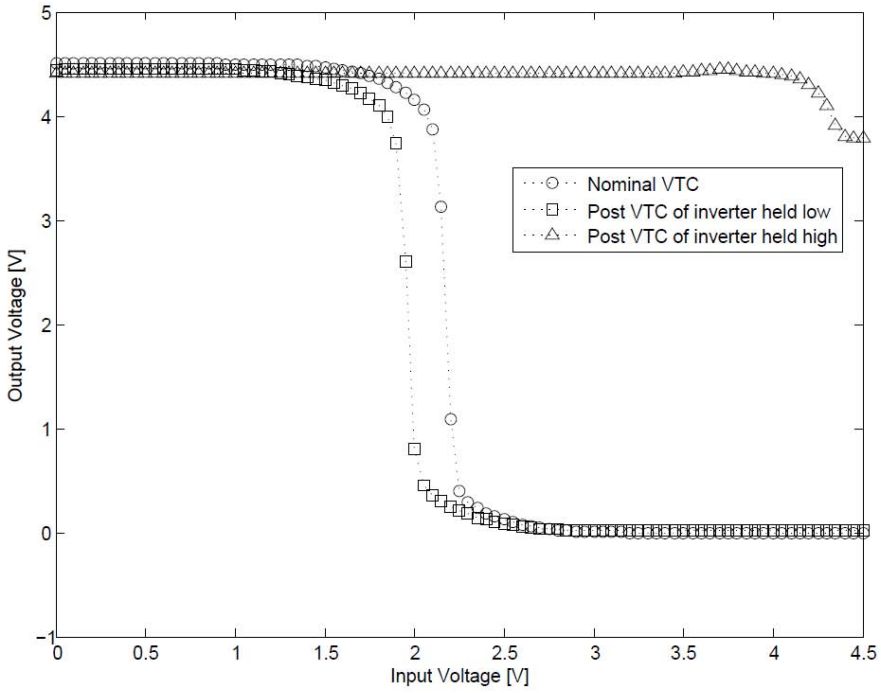

Figure 33. Post-VTC of outlier inverters, where the inverter held low began to fully turn on in the NMOS-on state at a lesser threshold voltage compared to the nominal. The inverter held high, NMOS-on state turned on even less and at a much higher V_{th}.

4.2.5 Capacitance Anomalous Measurement

One inverter input was held low with no RF applied and was irradiated from 10 nA to 2 μA until a change in the output was observed, as shown in Figure 34. The inverter response shows the current before an output step change; for example, the reading taken at 60 nA is the current at the time of the last measurement. The current was increased to 300 nA immediately after that measurement. The data taken at 2 μA was the last to be taken before a step change was observed, which is shown in Figure 35 (a). After the output changed, the beam was turned off. Several output measurements

were taken while the beam was off and it was observed that the NMOS-on side of the waveform was reverting to the pre-irradiation values. Figure 35, plot (b) shows that the waveform has shifted between pre-irradiation and the irradiation measurement.

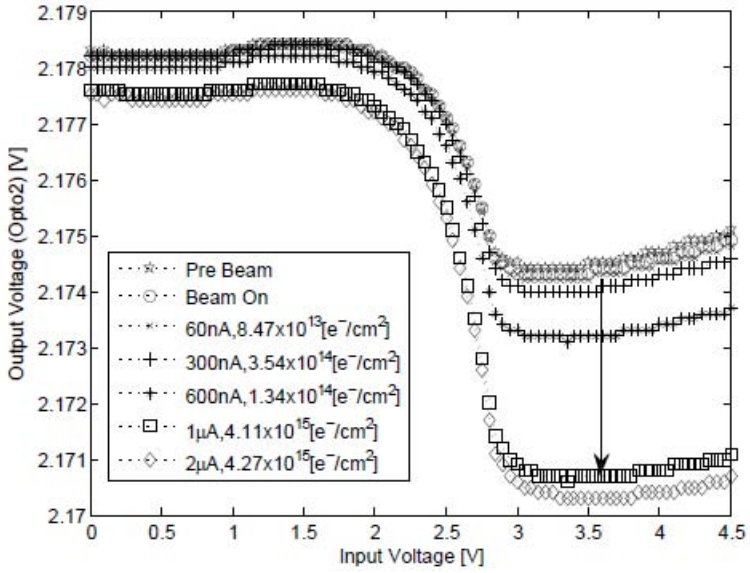

Figure 34. Inverter held low, first of three irradiations. A continuous negative output voltage shift is measured until a large change occurs.

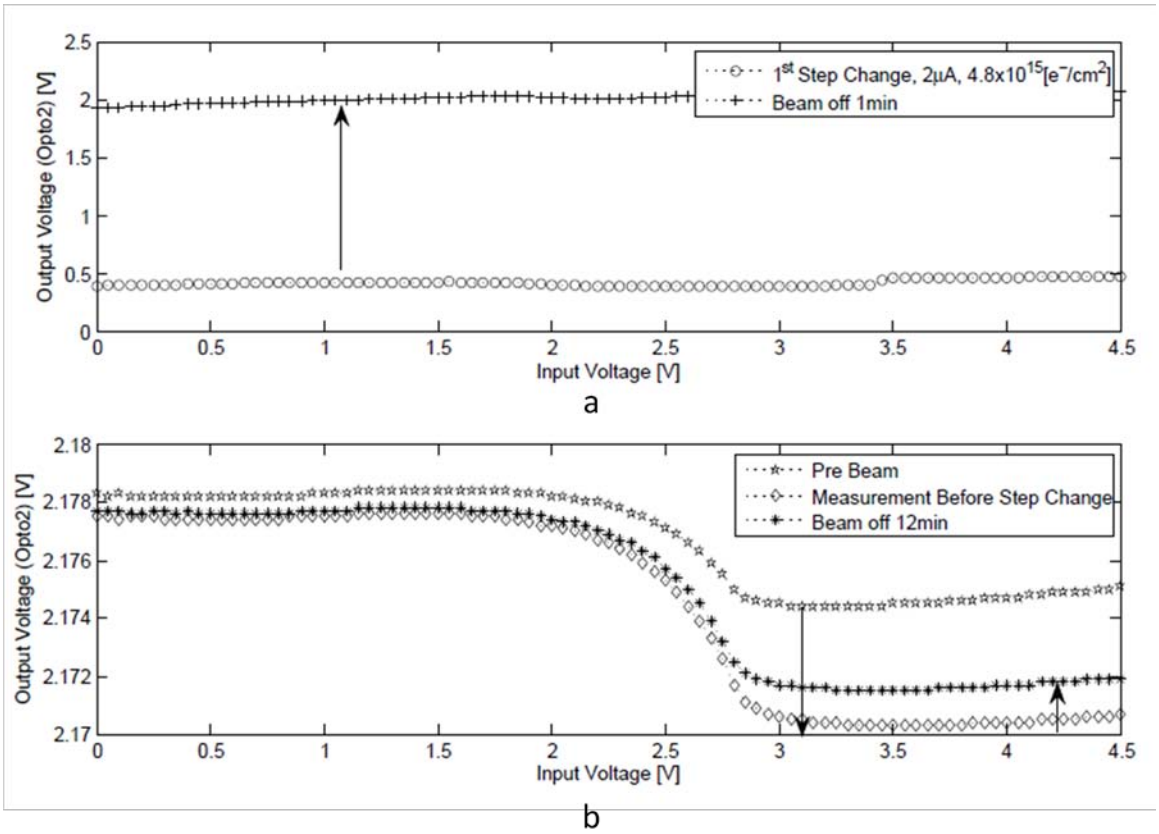

Figure 35. (a) depicts a large step change that occurred in the inverter, while (b) shows the shifting up of the waveform baseline after the beam is turned off.

After the waveform baseline voltage increased, the beam was turned on at 1μA, and a large downward step shift was immediately observed. The beam was turned off again and waveform baseline shifted up. The beam was turned on a third time at a lower current (100nA) and immediately the waveform shifted downward. Figure 36 presents these results. Plot (a) provides the waveform before the last irradiation, the shift after the beam was turned on and the accompanying output response. After turning the beam off, an increased to the waveform baseline is observed. Plot (b) in Figure 36, provides a comparison of the output waveform before irradiation, before the 3rd irradiation and the shift of the waveform after 18hrs.

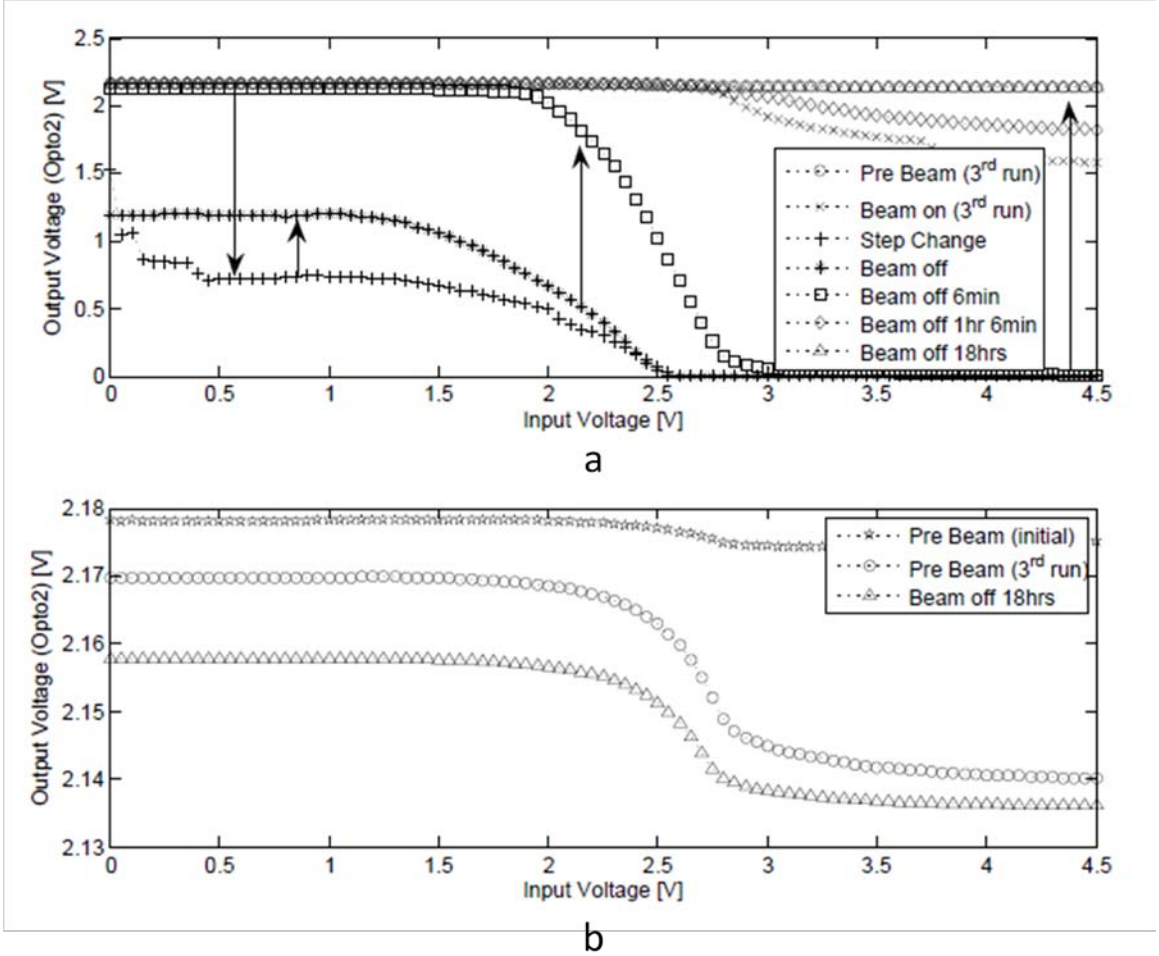

Figure 36. During the 3d irradiation, the inverter input was held low, after two previous step increases in output. (a) shows the waveform shift following irradiation and recovery. (b) shows the initial waveform before irradiation, waveform just prior to the 3rd irradiation, and the shifting of waveform toward the pre-irradiation position after 18hrs of post irradiation annealing.

Eighteen hours after irradiation, the battery in the test circuit was disconnected and reconnected. Figure 37 presents how the inverter responded to the disconnection/reconnection of the battery. Reconnection of the battery caused the waveform baseline, as observed by optoisolator 2, to be reduced. After the battery had been replaced, the waveform began to increase back toward the pre-irradiation waveform, as is indicated in Figure 37.

The waveform change indicates that the inverter capacitance has changed. Thus, the inverter output has a slow time response. A possible cause for this a diode type scenario, where the diode is forward biased while the capacitor discharges, but is in reverse bias while the capacitor charges.

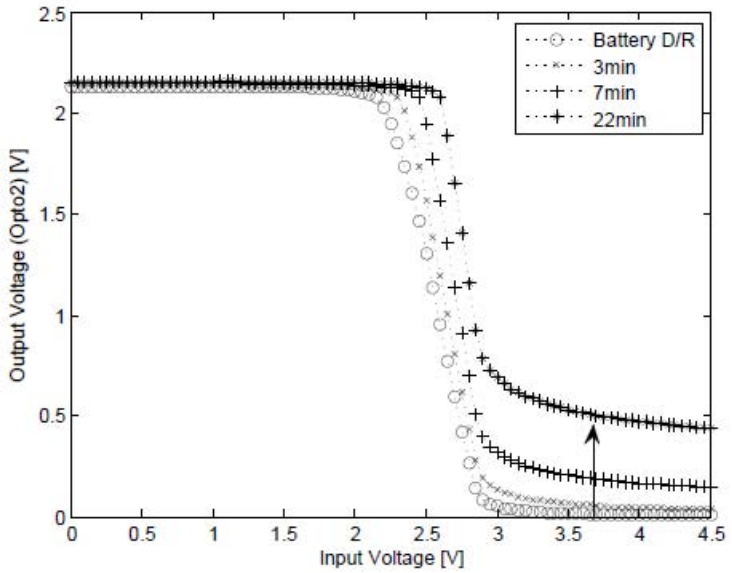

Figure 37. Battery is disconnected/reconnected in the test circuit. Upon the disconnection/reconnection the waveform is pulled down and then begins to slowly recovery towards its normal waveform as shown by the post battery reconnection plots of 3min, 7min and 22min.

Figure 38 shows the plot of the pre- versus post-VTC of this inverter. A negative V_{th} shift is observed along with a negative output voltage shift. After 25 days the post-VTC displays an annealing towards the nominal V_{th}. While the inverter was measured and held high, the PMOS-on state is turned fully on. However, when the inverter was measured while being held low the PMOS-on state does not fully turn on. Previous post-VTC high and low measurements were overlapped, however, in this case they have separated and the reason is not apparent.

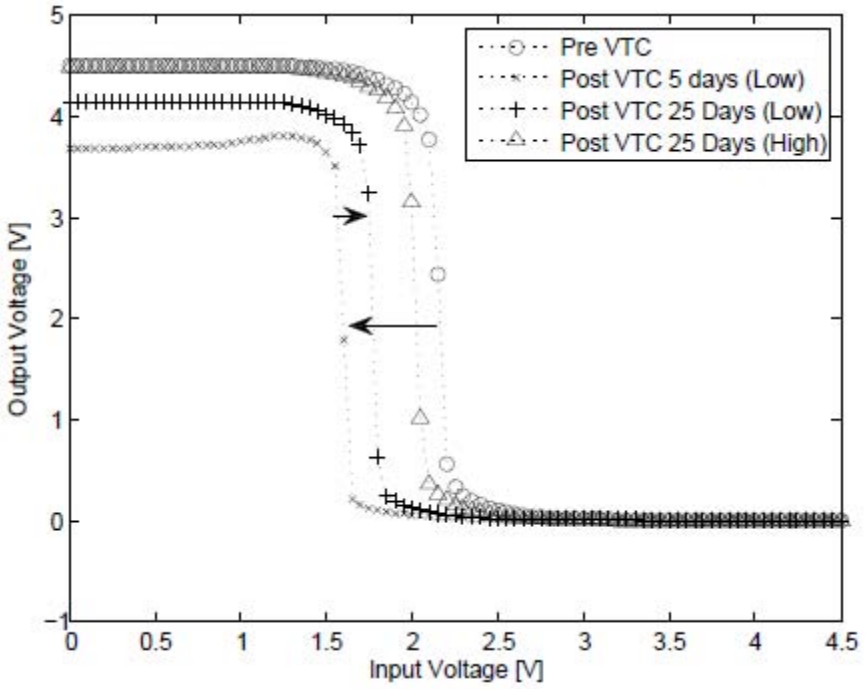

Figure 38. Pre-versus post-VTC of inverter held low with no RF applied. Post-VTC after 5 days presents a negative V_{th} shift, along with a decrease in output voltage. The inverter begins to anneal towards the nominal V_{th}, however a difference in operations of the devices is noted when held in a high vs low state.

4.2.6 RF Applied: Inverter Held Low

An RF signal was applied to an inverter with the inputs held low. The pre-versus post-VTC is shown in Figure 39. The inverter was irradiated for 1 hr 32 min to a fluence of 5.3×10^{15} [e^-/cm^2]. No sharp change in the output voltage occurred. There was a continuous reduction of the output voltage, as measured through optoisolator 2. The final ending fluence is lower than the inverters held high; however V_{th} shift (0.35±0.05 V) was not as great as those held high (1.65±0.05 V). The absence of the gate electric field increases the potential for initial recombination, which ultimately reduces the threshold voltage shift [23]. This was also observed in previous research as well [5].

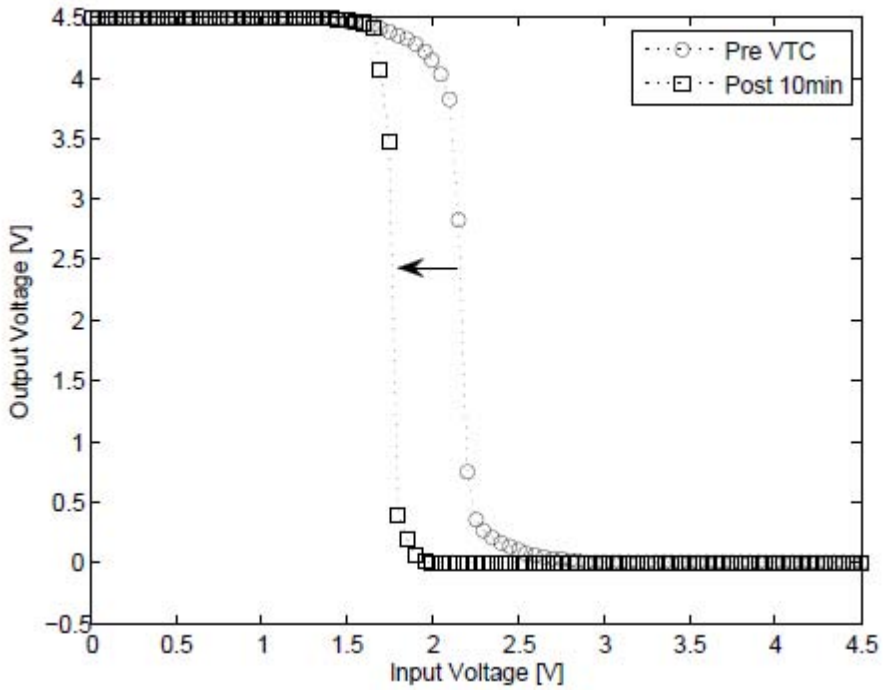

Figure 39. For the inverter with a low input and applied RF signal, a threshold voltage shift of 0.35 ±.05 V was observed. No step change in output during irradiation was observed as with some inverters with inputs held high.

4.3 Inverter Response to RF and Electron Irradiation using Test Circuit B

Test circuit B was developed to resolve the issue of the NMOS-on side of the waveform floating, as in Figure 24-Figure 39. The isolated side of the optoisolators and the inverter were grounded to the Dynamitron ground, which brought the NMOS-on side of the waveform down to zero volts, allowing for a larger view-window. The waveform shift in the previous section may not only be affected by the radiation, but also charge build up on the inverter. This also helps explain the annealing that occurred after the beam was turned off.

The following section presents the results of test circuit B's measurements. While the viewing window is larger (due to grounding the optoisolator 1 and the inverter), the overall radiation affects in test circuit A are comparable to those of test circuit B.

4.3.1 Electron Irradiation: Inverters Held High

Inverters with a nominal VTC were held high during irradiation and test circuit B was used. The same procedure was used as in section 4.2.2. Results displayed in Figure 40, are similar to those in test circuit A, but instead of the output voltage on the NMOS-on side of the waveform steadily decreasing, the PMOS-on side shifts downward.

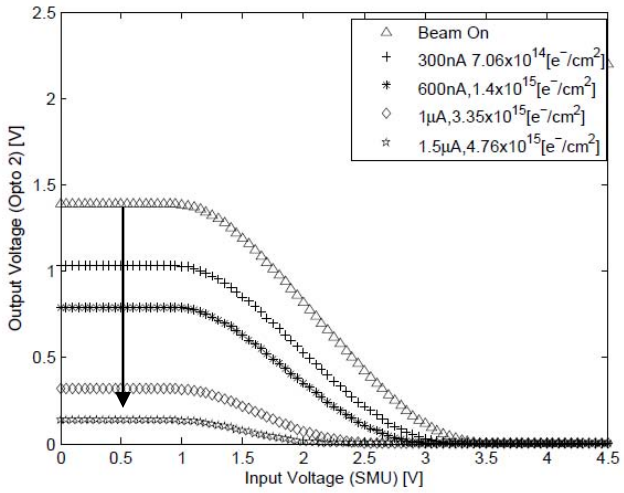

Figure 40. Inverter held high with no RF applied, irradiated at different current densities. A downward output voltage trend occurs on the PMOS-on state.

Figure 41 shows the final two fluence levels, displaying the continued downward shift of the waveform. Figure 42 is the plot of the pre-versus post-VTC of the inverter. Results show a good correlation between test circuit A and B, displaying a continuous decrease in output voltage. While test circuit A's NMOS-on side would shift upward after the beam was turned off, neither the PMOS-on nor the NMOS-on side of the waveform as viewed by test circuit B shifted. This indicates that the upward shift as seen by test circuit A was due to charge accumulation on the inverter.

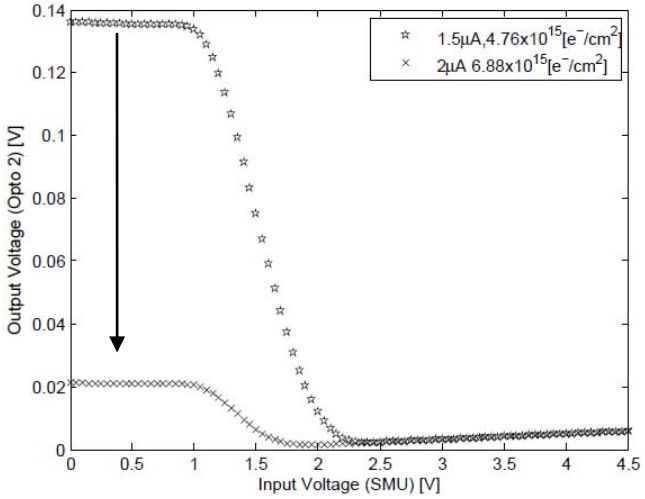

Figure 41. Inverter held high with no RF applied, presents the final two fluence levels during irradiation.

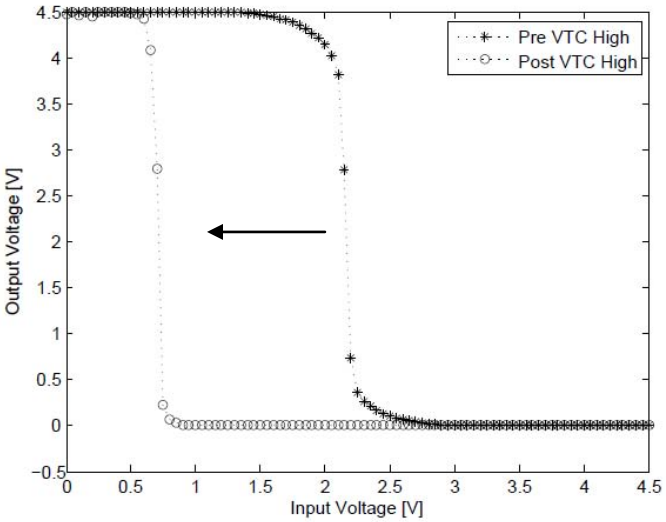

Figure 42. Pre-versus post-VTC of inverter held high with no RF applied, presents a negative V_{th} shift.

4.3.2 Total Dose versus Total Dose Rate Effect

In order to answer the question on whether the effects measured were from total dose or dose rate, the following procedure was followed. Three inverters, all having the nominal VTC characteristic, were irradiated at the same fluence level of 7.06×10^{14} [e^-/cm^2], but irradiated at different fluxes. Figure 43-Figure 47 display the correlation; the results show that at these fluxes an absorbed dose effect is occurring rather than a dose rate effect.

The inverter in Figure 43 was held high and the current applied was held constant at 300 nA, with an ending flux of 3.56×10^{11} [e^-/cm^2 sec]. A drop in output voltage of 0.4 V was noted. A post-VTC was not acquired at this fluence level due to the total shot being irradiated at 2 μA.

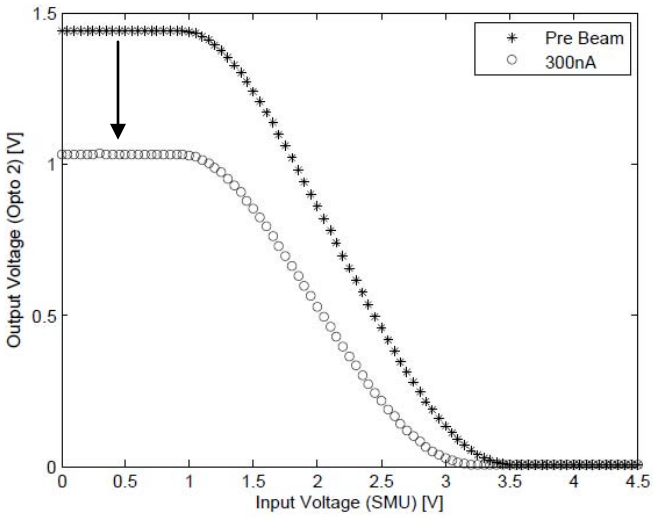

Figure 43. Inverter held high using test circuit B, current applied at 300 nA. A fluence of 7.06×10^{14} [e^-/cm^2] was applied at a flux of 3.56×10^{11} [e^-/cm^2 sec].

The same setup was used for another inverter, however this time the current was held constant at 600 nA. Figure 44 and Figure 45 display the in-situ measurements and

the pre-versus post-VTC measurements. A flux of 6.663×10^{11} [e^-/cm^2 sec] was used. Similar input/output voltage shifts were noted. An output voltage shift of 0.43 V as seen by optoisolator 2 was observed. The pre- versus post-VTC showed a shift of 0.3 V. A difference in initial output voltage is noted in Figure 43 versus Figure 44. This difference was attributed to the dissipation in the battery power to the inverter. Although the starting points were slightly different, their waveform drops are similar in magnitude.

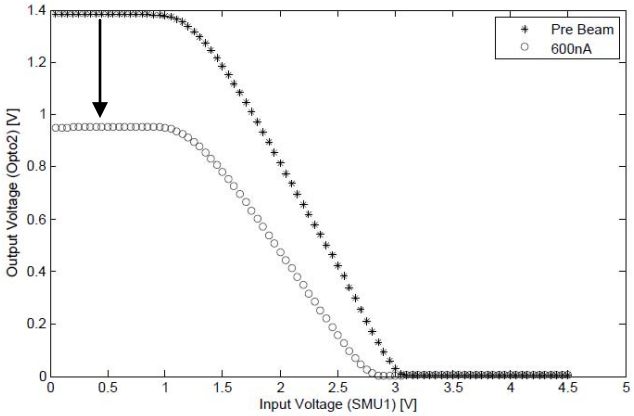

Figure 44. Result of measurement when the inverter is held high with a constant current of 600 nA. The same fluence of 7.06×10^{14} [e^-/cm^2] was obtained as in the previous case, but a flux of 6.663×10^{11} [e^-/cm^2 sec] was achieved.

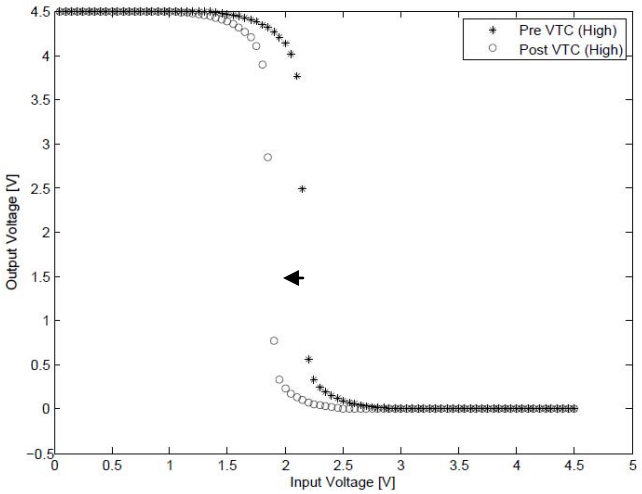

Figure 45. Pre-versus post-VTC of inverter being irradiated at 600 nA, a 0.3 V negative V_{th} was observed

A 3rd inverter was irradiated at a current of 1 μA. The same procedures were followed. Figure 46 and Figure 47 display the results for a flux of 1.7×10^{12} [e^-/cm^2 sec]. Figure 46 shows an output voltage drop of 0.457 V. The pre-versus post-VTC plot of Figure 47 also showed negative threshold voltage shift of 0.3 V.

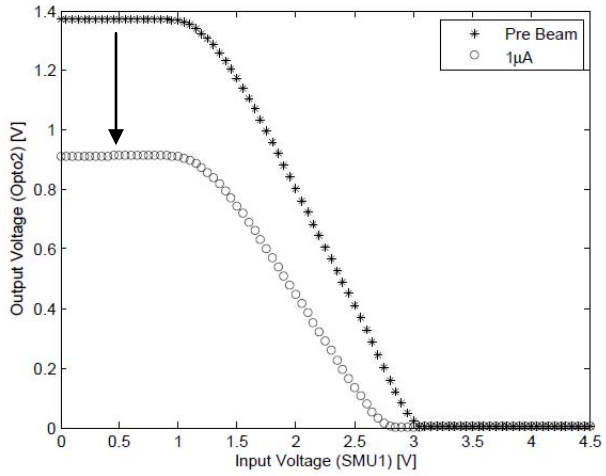

Figure 46. Inverter held high with a constant current applied at 1 A. The same fluence of 7.06×10^{14} [e^-/cm^2] was obtained as in the previous two cases, but a flux of 1.7×10^{12} [e^-/cm^2 sec] was achieved.

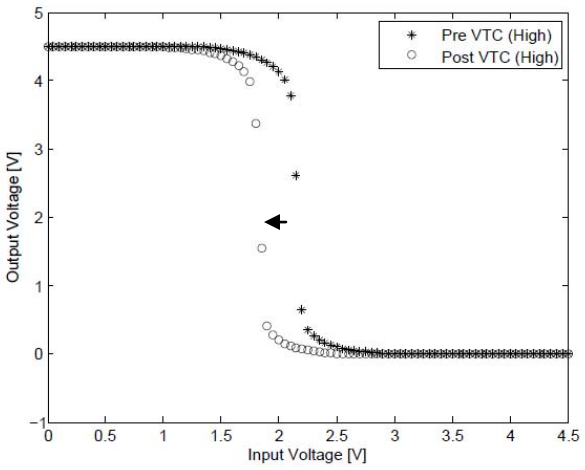

Figure 47. Pre-versus post-VTC of inverter being irradiated at 1 A, a similar 0.3 V negative V_{th} was observed.

The constant increase in flux, as seen in Figure 43 and Figure 47, with no increase in V_{th} shift, indicates that at these flux levels the response was from total dose. A similar shift was noted throughout each measurement, which indicated that the flux had little effect on the inverter.

4.3.3 Combine RF and Electron Irradiation: Inverters Held High

The procedure used in section 4.3.2 was repeated, but a 500 kHz RF signal was applied to each inverter. The measurements did not indicate any influence of the RF signal on the inverter. A distortion of the waveform occurred as shown in Figure 48, but no direct correlation between increased/decreased anneal time of EHPs can be determined with the collected data. Figure 49 presents one of the irradiation, where the current rate was at 300 nA. A downward output voltage shift of 0.45 V and a threshold voltage shift of 0.3 V were measured. At currents of 600 nA and 1 μA similar shifts were observed.

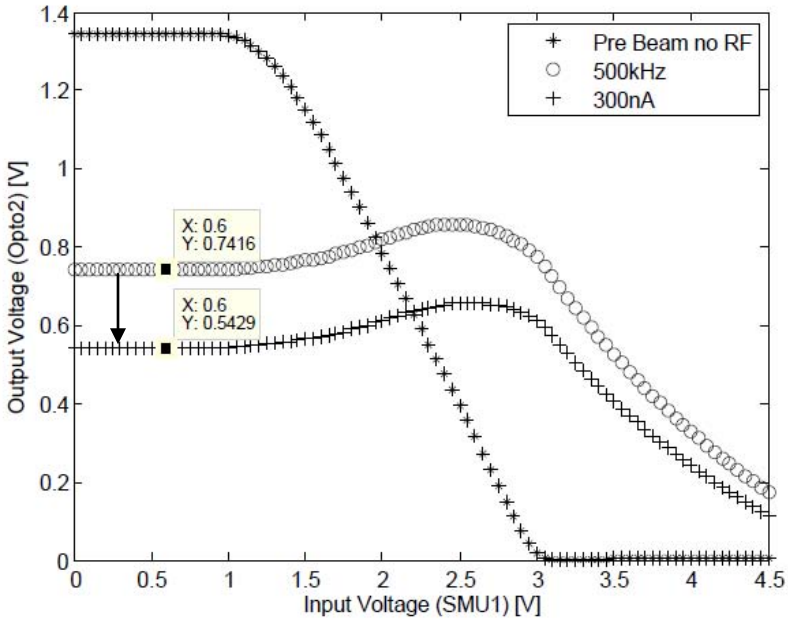

Figure 48. Inverter held high, presents pre-beam with no RF, a coupled RF signal of 500kHz reduces and distorts the waveform. A beam current of 300 nA was applied while the RF signal was coupled onto the inverter.

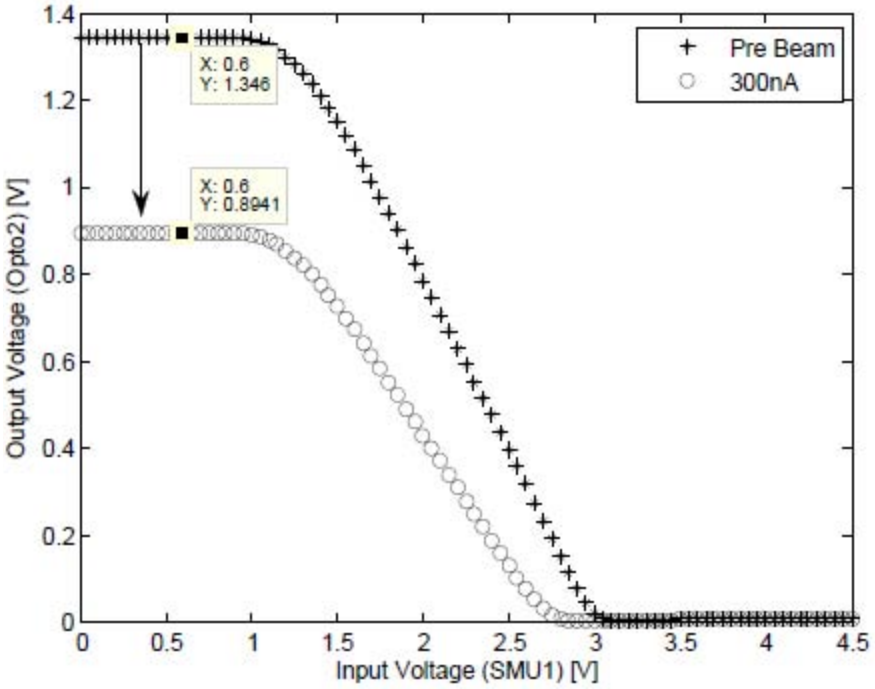

Figure 49. Pre-versus post-irradiation with the RF signal and beam current removed. Similar shifts occurred as compared to those inverters with no RF applied.

4.4 Decrease in Output Voltage as seen by Optoisolator 2

The decrease in output voltage as seen by optoisolator 2 may be described via two mechanisms. In-order for the output voltage on optoisolator 2 to decrease, the output from the inverter must also decrease in voltage. V_{DD} is what controls the level of output voltage on the inverter. Therefore, V_{DD} is the first mechanism. During an irradiation, the battery powering V_{DD} began to decrease in voltage, by as much as a 0.3 V. While the dissipation of voltage accounts for some of the output drop, it is a small portion of it. A test was performed to validate that the battery's voltage drop was not the main cause of the output voltage drop. A battery with a start voltage of 9.36 was connected to the inverter and measured. That battery was then replaced with two other batteries, one at 8.59 V and the other at 7.99 V. (Note that both replacement batteries are at a much lower

voltage than what was lost during irradiation.) The results are displayed in Figure 50. From 9.36 V to 7.99 V a downward shift of 0.55 V was observed. In Figure 41, a much larger output voltage shift of 1.38 V was observed, while a much smaller battery loss of 0.36 V occurred.

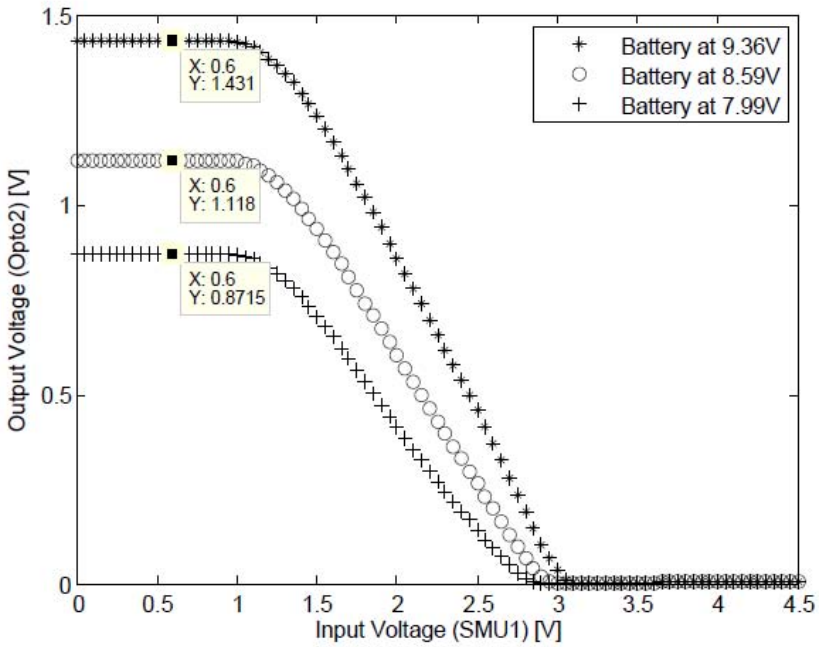

Figure 50. A comparison using different batteries at various V_{DD} voltages, indicating that while the battery decreases voltage during an in-situ measurement it is not the key mechanism that caused the decrease in output voltage.

The second mechanism is related to V_{DD}, in which the downward output voltage shift is caused within the PMOS transistor. The PMOS does not fully turn on, therefore the full potential of V_{DD} is not applied. This is presented in previous research, as shown in Figure 5, a downward output voltage shift is seen in the VTC curve. While the downward output voltage shift has not been captured in the post-VTC measurement of this research, it does not disprove that a downward output voltage shift was occurring

during the in-situ measurements. An explanation of this is in previous research, the inverter was held high the entire time, in-situ and post measurements. However, for this research, the inverter was held high during the in-situ measurements, but in order to take the post measurement, the battery needed to be disconnected in order to connect the inverter directly to the Keithley 4200. The disconnection of V_{DD} power to the inputs of the inverter allowed for recombination of the trapped positive charges in the oxide to occur in the PMOS, thus allowing for the output voltage to shift positive towards the nominal VTC position.

It is possible to show that the output voltage shift, as measured though optoisolator 2, is caused from ionizing radiation. This is done by comparing the charge per unit area produced by the flux of the electron beam to an estimate of the charge per unit area created in the oxide. The total charge is found using

$$Q = \int i \, dt \tag{0}$$

where Q is the charge per unit area $\left[\frac{C}{cm^2}\right]$ from the beam, i is the current of the beam and t is the length of irradiation time [s]. To calculate $C_{ox,}$ the capacitance per unit area in the oxide $\left[\frac{F}{cm^2}\right]$, equation (9) is used, here, $_{ox}$ is the permittivity of the SiO_2 and t_{ox} is the thickness of the oxide layer.

$$C_{ox} = \frac{\varepsilon_{ox}}{t_{ox}} \tag{0}$$

From this, one can then find the charge per unit area by

$$Q_s = V_o C_{ox} \tag{0}$$

where, Q_s is the charge per unit area of the oxide and V_o is the voltage shift seen by optoisolator 2. However, the charge created in the oxide was an order of magnitude lower than the potential charge created by the flux of the beam. If initial recombination accounts for the discrepancy in magnitude, it is plausible to conclude that the downward output voltage shift is due to positive trapped charge in the oxide.

V. Conclusions and Recommendations

The test circuit created for this research provided the unique opportunity to measure ionizing radiation effects on the inverter during electron irradiation. It also allowed for the ability to note when critical damaging factors occurred to the inverter while in-situ. These damaging factors were observed as ionizing radiation and current or HV spikes from the electron beam.

5.1 Summary of Results

Negative V_{th} shifts were consistent among the various irradiations. These shifts correspond to what was observed in previous research [5]. The negative V_{th} shifts occur due to the positive trapped charge in the oxide and interface traps causing the NMOS to turn on sooner. What could not be observed, as shown in previous research, was the PMOS not turning on to the full potential of V_{DD}, thus decreasing the output voltage. This may have occurred in the inverter, but was missed due to the inability to take a post irradiation measurement and while continuously keeping the inverter held high. Switching from the test circuit to a direct connection of the Keithley 4200 caused the inputs held high to be disconnected, thus, allowing for recombination to occur in the PMOS transistor.

Current spikes were problematic during early irradiation, which may have caused inadvertent degradation of the inverters. However, having the capability to view the inverters in-situ, allows one to record and observe these effects, which provides the potential for future analyses of the pulses' overall impact to an inverter. Inverters that did not maintain a nominal VTC characteristic showed more responsive reaction to the

irradiation. This may indicate that outliers might be able to be corrected through the process of light ionization.

RF applications appeared to affect the recovery of the inverters as measured in test circuit A. However, the results from test circuit B do not verify this. Therefore, it is possible that the floated inverter was acquiring charge from the beam and the RF signal was holding it there for a longer time. Once grounded, the charge was able to quickly find the lower potential and move away from the inverter.

Similar results were obtained as noted in previous research [5]. Such as a total absorbed dose effect versus dose rate. Also observed were the larger negative V_{th} shifts when the inverter was held high, as compared to low.

5.2 Future Recommendations

While the test circuit was only able to measure a small portion of what was occurring in an inverter during an in-situ measurement, the information that came out of this research provides a baseline for future in-situ measurements using an electron accelerator. Some recommendations for future research are: measuring the temperature of the device, changing the power and frequency of the RF signal and developing a more efficient data collection system.

Temperature during irradiation measurements was not measured, although the inverters were cooled via the cold head. Research has shown that heating affects the shift in V_{th} of MOS transistors [6]. It would be beneficial to record the temperature of the inverter during irradiation to rule out if joule heating affects any of the results.

A better signal coupling method is needed to ensure the measured signal strength reaches the inverter. This could be done by creating a cold head, in which an SMA cable could be passed through, thus allowing for near direct connection of the SMA cable to the inverter. Once a better technique is found for coupling the RF signal into the inverter, various RF frequencies and power could be examined.

It would be beneficial for a system to automatically collect the data from the electron accelerator. Important data include: counts from the current integrator, full scale current, vacuum pressure, and beam high voltage. If a program continuously collected this information, it would give a better understanding of what may be occurring in an inverter when a large change is observed. It would help rule out any anomalies that may be produced by the electron accelerator that are not direct effects from the radiation.

From an experimental standpoint, it would be favorable to re-address certain results obtained from this research. Further investigations of dose versus dose rate are still needed for larger fluxes. Another area of interest is the effect of the inverter state during irradiation and post irradiation anneal. In-order to gain a better understanding of what was occurring within the components of the inverter; these results should be recreated and examined.

Appendix A. Experimental Equipment

Item	Quantity
Keithley 4200	1
Mini-Circuits ZX85-12G (Bias T)	1
Mini-Circuits 4N35 (Optoisolator)	2
Mini-Circuits ZHL-32A (RF Amplifier)	1
Agilent E4438C ESG Vector Signal Generator	1
HP87720C Vector Network Analyzer	1
CD4069UB CMOS hex inverter devices	25
20’ SMA cables	2
6’ SMA cable	1
45’ CAT 5	1
Signal Box	1
Test Circuit	1
9V Batteries	10
4’ BNC	1
Mastech HY3006D (DC Power Supply)	1
HP 8563A Option 026 (Spectrum Analyzer)	1

Bibliography

[1] John Mueller, "Policy and Opinion in the Gulf War," University of Chicago Press, Chicago, 1994.

[2] "Commander's Handbook on the Law of Armed Conflict," Air Force Pamphlet 110-34, 1980.

[3] Mats G. Backstrom and Karl Lovstrand, "Susceptibility of Electronic Systems to High-Power Micorwaves: Summary of Test Experience," *IEEE Transactions on Electromagnetic Compatibility*, vol. 46, no. 3, August 2004.

[4] T. P. Ma and Paul V. Dressendorfer, *Ionizing Radiation Effects in MOS Devices and Circuits*. Hoboken: John Wiley and Sons, Hoboken, 1989.

[5] Nicholas A. Estep, "High Power Microwave (HPM) and Ionizing Radiation Effects on CMOS Devices," School of Engeering, Air Force Institute of Technology (AU), Wright-Patterson AFB OH, M.S. Thesis AFIT/GE/ENG/10-08, 2010.

[6] Adel Sedra and Kenneth C. Smith, *Microelectronic Circuits*. New York: Oxford University Press, 2004.

[7] B. Wilson. (2008, May) CMOS Logic, Connexions Web site. [Online]. "http://cnx.org/content/m1029/2.12/"

[8] R. K. Chauhan, S. Dasgupta, and P. Chakrabarti, "Influence of ionizing radiation on the performance of CMOS inverter," *Microelectronics*, vol. 32, pp. 615-620, February 2001.

[9] S.M. Sze, *Semiconductor Devices Physics and Technology*, 2nd ed. Hoboken: John Wiley & Sons, Inc., 2002.

[10] D.C. Giancoli, *Physics for Scientists and Engineers*. Upper Saddle River: Prentice Hall, 2000.

[11] J. Lochner. (2010, February) Electromagnetic Spectrum, Measuring the electromagnetic spectrum. [Online].

"http://imagine.gsfc.nasa.gov/docs/science/know_l1/emspectrum.html"

[12] Gary Farlow, Associate Professor of Physics, Wright State University, Dayton OH, Personal Interview, Dec 2010.

[13] A. Holmes-Siedle and L. Adams, *Handbook of Radiation Effects*. New York: Oxford, 2007.

[14] R Hoad, D. Carter, and S.P. Watkins, "Trends in EM susceptibility of IT equipment," *IEEE Trans. Electromagn. Compat*, vol. 43, pp. 391-396, August 2004.

[15] D. Pozar, *Microwave Engineering*.: Addison-Wesley, 1993.

[16] W. A. Radasky, C. E. Baum, and M. W. Wik, "Introduction to the Special Issue on High-Power Electromagnetics (HPEM) and Intentional Electromagnetic Interference (IEMI)," *IEEE Transactions on Electromagnetic Compatibility*, vol. 46, no. 3, pp. 314-321, August 2004.

[17] R. A. Venugopala, A. Roy, A. Paithankar, and P. Roh, "Electromagnetic Interference by High Power Microwaves," in *Mumbai: Bhabha Atomic Research Centre*, 2002.

[18] P. Dolan and S. Glasstone, *The Effects of Nuclear Weapons*, 3rd ed. Washington D.C., 1977.

[19] (2010, November) Dynamitron Operating Principles. [Online]. "http://www.iba-industrial.com/accelerators/dynamitro-operating-principles"

[20] H. J. Barnaby, "Total-Ionizing-Dose Effects in Modern CMOS Technologies," *Nuclear Science*, vol. 53, no. 6, pp. 3103-3121, December 2006.

[21] James Petrosky, Radiation Effects on Electronic Devices.

[22] Klaus G. Kerris, "Practical Dosimetry for Radiation Hardness Testing," in *Defense Nuclear Agency*, 1992.

[23] J.H. Hubbel and S.M. Seltzer. (2010, October) Table of X-ray Mass Attenuation Coefficients and Mass Energy-Absorption Coefficients. [Online].

"http://www.nist.gov/pml/data/xraycoef/index.cfm"

[24] G.Bowman, C. Brucker and S. Seehra, "Study to Establish Data Sheets for CMOS Devices in Space and Nuclear Applications," *IEEE Transactions on Nuclear Science*, vol. NS-32, no. 6, pp. 4244-4249, December 1985.

[25] Texas Instruments CD4069UB Hex Inverter Data Sheet, 2003.

[26] Dynamitron Accelerator Operation and Service Manual.

[27] J.S. Blaemore, *Solid State Physics*. Philadelphia: Suanders Co., 1974.

[28] Mini-Circuits Coaxial Bias-Tee Data Sheet.

[29] B.S. Ziebro, D.C. Look, J.W. Hemsky, and W. Rice, "In situ Hall-effect system for real-time electron-irradiation studies," *American Institute of Physics*, vol. 61, pp. 192-194, January 1990.

[30] P. Scherz, *Practical Electronics for Inventors*, 2nd ed. New York: McGraw-Hill, 2007.

[31] Fairchild Semiconductor General Purpose 6-Pin Phototransistor Optocouplers Data Sheet.

REPORT DOCUMENTATION PAGE

Form Approved
OMB No. 074-0188

1. REPORT DATE *(DD-MM-YYYY)*	2. REPORT TYPE	3. DATES COVERED *(From – To)*
24-03-2011	Master's Thesis	Jun 2010-Mar 2011

4. TITLE AND SUBTITLE

Combined Effects of Radio Frequency and Electron Radiation on CMOS Inverters

5a. CONTRACT NUMBER

5b. GRANT NUMBER

5c. PROGRAM ELEMENT NUMBER

6. AUTHOR(S)

Dahl, Kristofer, R., 2nd Lieutenant, USAF

5d. PROJECT NUMBER

5e. TASK NUMBER

5f. WORK UNIT NUMBER

7. PERFORMING ORGANIZATION NAMES(S) AND ADDRESS(S)

Air Force Institute of Technology
Graduate School of Engineering and Management (AFIT/EN)
2950 Hobson Way
WPAFB OH 45433-7765

8. PERFORMING ORGANIZATION REPORT NUMBER

AFIT/GNE/ENP/11-M03

9. SPONSORING/MONITORING AGENCY NAME(S) AND ADDRESS(ES)

National Nuclear Security Agency –
Attention: Maj Paul Adamson
Office of Technology Maturation and Stockpile Assessment
NA-124 U.S. Department of Energy
NNSA 1000 Independence Avenue
SW Washington DC 20585

10. SPONSOR/MONITOR'S ACRONYM(S)

11. SPONSOR/MONITOR'S REPORT NUMBER(S)

12. DISTRIBUTION/AVAILABILITY STATEMENT

APPROVED FOR PUBLIC RELEASE; DISTRIBUTION UNLIMITED

13. SUPPLEMENTARY NOTES

14. ABSTRACT

This research examines the measurement methodology, and the results of, the combined effects of electron and radio frequency irradiation (500kHz) on a CMOS Hex Inverter, CD4069UB. There have been many studies in recent years on the effects of electron radiation and electromagnetic interference on integrated circuits, however the combined effects have not been measured. A major obstacle for in-situ electron irradiation experiments is the over current hazard that exists to measurement equipment that comes from taking real-time, in-situ measurements. To overcome this, a test circuit was designed and built to allow for real-time in-situ measurement of the output voltage, current and the inverter power. This test circuit provides real–time measurement of the inverter's threshold voltage with respect to electron dose. During this research pre- and post-electron irradiation measurements (1MeV electrons with fluences up to $8x10^{15}[e^{-}/cm^{-2}]$ at various fluxes), combined with RF were made using a continuous 500kHz RF signal coupled into the inverter input. The data provided insight into the total dose effect as opposed to a dose rate effect on the inverter. A significant negative threshold voltage shift was observed along with a limited amount of annealing. Inverters that were outliners from nominal VTC characteristics displayed an enhanced failure rate. The combined effects of radio frequency are inconclusive, but indicate that the RF decreases post irradiation annealing.

15. SUBJECT TERMS

Real time in-situ measurements, electron radiation, RF radiation

16. SECURITY CLASSIFICATION OF:			17. LIMITATION OF ABSTRACT	18. NUMBER OF PAGES	19a. NAME OF RESPONSIBLE PERSON
a. REPORT	b. ABSTRACT	c. THIS PAGE			Dr. James C. Petrosky
U	U	U	UU	92	19b. TELEPHONE NUMBER *(Include area code)* (937)255-6565, ext 4562 (james.petrosky@afit.edu)

Standard Form 298 (Rev. 8-98)
Prescribed by ANSI Std. Z39-18